

TA7  
C6  
CER 66/17

copy 2

B-479

ENGINEERING RESEARCH

JUL 1 1969

FOOTHILLS READING ROOM

Technical Report

SIMULATION OF ATMOSPHERIC MOTION BY  
WIND-TUNNEL FLOWS

J. E. Cermak, V. A. Sandborn, E. J. Plate  
G. H. Binder, H. Chuang, R. N. Meroney and S. Ito

Prepared under

U. S. Army Research Grant DA-AMC-28-043-G20  
U. S. Army Materiel Command  
Washington 25, D. C.



Property of Civil Engineering  
Dept. Foothills Reading Room

Received 5-27-66

**FLUID MECHANICS PROGRAM  
ENGINEERING RESEARCH CENTER  
COLLEGE OF ENGINEERING  
COLORADO STATE UNIVERSITY  
FORT COLLINS, COLORADO**

Technical Report

SIMULATION OF ATMOSPHERIC MOTION BY  
WIND-TUNNEL FLOWS

J. E. Cermak, V. A. Sandborn, E. J. Plate  
G. H. Binder, H. Chuang, R. N. Meroney and S. Ito

Prepared under

U.S. Army Research Grant DA-AMC-28-043-G20  
U.S. Army Materiel Command  
Washington 25, D. C.

Fluid Dynamics and Diffusion Laboratory  
College of Engineering  
Colorado State University  
Fort Collins, Colorado

May 1966

CER66JEC-VAS-EJP-GJB-HC-RNM-SI17



U18401 0574336

## ABSTRACT

The objective of this study was to survey and compile information and experience obtained by the authors with respect to simulation of atmospheric motions by wind-tunnel flows. These notes are restricted to atmospheric phenomena in the lower 1000 m of the atmosphere as determined by the interests of the staff and the capabilities of the wind tunnels associated with the Fluid Dynamics and Diffusion Laboratory at Colorado State University.

TABLES

<u>Table</u>		<u>Page</u>
1	Performance Characteristics of the Meteorological and Low-Speed Wind Tunnels . . . . .	17
2	Magnitudes of Turbulent Dissipation for Atmospheric and Laboratory Flow Conditions . . . . .	54
3	Average Values for Universal Spectral Energy Distribution Function Obtained from Meteorological Wind Tunnel Data . . . . .	55

## FIGURES

<u>Figure</u>		<u>Page</u>
1	Boundary characteristics for flat plate in the meteorological wind tunnel . . . . .	73
2	Boundary characteristics for flexible roughness in the meteorological wind tunnel . . . . .	74
3	Boundary characteristics for gravel and flexible roughness in the meteorological wind tunnel . . . . .	75
4	Average size turbulent eddies in meteorological wind tunnel . . . . .	76
5	Average size turbulent eddies in meteorological wind tunnel . . . . .	77
6	Boundary characteristics for flat plate under unstable conditions in the meteorological wind tunnel . . . . .	78
7	Distribution of Richardson number with height in the atmosphere . . . . .	79
8	Distribution of Richardson number with height in the meteorological wind tunnel . . . . .	80
9	Non-dimensional velocity profiles above crop: logarithmic law . . . . .	81
10	Field data in canopy . . . . .	82
11	Comparison of the experimental data with the universal wind profile of Monin and Obukhov . . . . .	83
12	Log-linear law on logarithmic scale for stable flow .	84
13	Log-linear law on logarithmic scale for unstable flow . . . . .	85

FIGURES - Continued

<u>Figure</u>		<u>Page</u>
14	Model-prototype mean flow correlation, Candlestick Ball Park (Ref. 4) . . . . .	86
15	Model-Prototype mean flow correlation, Point Arguello: (comparison of cloud movements from Hondo Canyon for 340 <sup>0</sup> winds) . . . . .	87
16	Typical ammonia trace on San Nicolas Island model, as mounted in meteorological wind tunnel . . . . .	88
17	Titanium-tetra chloride smoke trails in wake of San Nicolas Island model . . . . .	88
18	Smoke patterns over San Nicolas Island prototype . . . . .	89
19	Comparison of spectra measurements from the Army meteorological wind tunnel, an ocean tidal channel and air flow over the sea surface . . . . .	90
20a	Normalized energy spectra - smooth surface . . . . .	91
20b	Normalized energy spectra - gravel and flexible roughness . . . . .	92
20c	Normalized energy spectra - flexible roughness . . . . .	93
21	Total turbulent energy dissipation in boundary layers . . . . .	94
22a	Evaluation of the large scale turbulence . . . . .	95
22b	Evaluation of the large scale turbulence . . . . .	96
22c	Evaluation of the large scale turbulence . . . . .	97
23	Spectrum of horizontal gustiness in high winds . . . . .	98

FIGURES - Continued

<u>Figure</u>		<u>Page</u>
24	Turbulent intensity of vertical velocity component versus Richardson number . . . . .	99
25	The exponent-of-distance $m_{cp}$ for attenuation of maximum ground-level concentration as a function of distance and source height resulting from a point source in a neutral boundary layer . . . . .	100
26	Downwind variation of dilution and concentration . .	101

## SYMBOLS

Symbol		
$C = \bar{C} + c$ $C' = \bar{C}' + c'$	$\left. \vphantom{\begin{matrix} C \\ C' \end{matrix}} \right\}$	Concentration - $\left\{ \begin{array}{l} \text{Instantaneous and mean values} \\ \text{Dimensionless form} \end{array} \right.$
$C_v$		Specific heat at constant volume
$C_p$		Specific heat at constant pressure
$C_f$		Skin friction coefficient
Eu		Euler number
Fr		Froude number
g		Body force, i. e. gravitational magnetic, etc.
k		Thermal conductivity
$K_h$		Exchange coefficient for heat (see Eq. 4-5)
$K_m$		Exchange coefficient for momentum (see Eq. 4-5)
L		Characteristic length
m		Constant (see Eq. 4-6)
$P = \bar{P} + p$ $P' = \bar{P}' + p'$	$\left. \vphantom{\begin{matrix} P \\ P' \end{matrix}} \right\}$	Pressure - $\left\{ \begin{array}{l} \text{Instantaneous and mean values} \\ \text{Dimensionless form} \end{array} \right.$
Pr		Prandtl number
r		Radius
Ro		Rossby number

## SYMBOLS - Continued

### Symbol

$Re$	Reynolds number	
$Ri$	Richardson number	
$\left. \begin{aligned} T &= \bar{T} + \theta \\ T' &= \bar{T}' + \theta' \end{aligned} \right\}$	Temperature -	$\left\{ \begin{aligned} &\text{Instantaneous and mean values} \\ &\text{Dimensionless form} \end{aligned} \right.$
$t$	Time	
$u^*$	Friction velocity	
$U_a$	Ambient velocity	
$\left. \begin{aligned} U_i &= \bar{U}_i + u_i \\ U &= \bar{U} + \underline{u} \\ U'_i &= \bar{U}'_i + u'_i \end{aligned} \right\}$	Velocity -	$\left\{ \begin{aligned} &\text{Instantaneous and mean values} \\ &\text{Vector form} \\ &\text{Dimensionless form} \end{aligned} \right.$
$V$	Scaling velocity	
$x$	Longitudinal distance	
$z$	Distance perpendicular to boundary	

### Greek Symbols

$\alpha$	Constant (see Eq. 4-7)
$\beta$	Monin-Obukhov linear velocity coefficient
$\gamma$	Specific weight
$\gamma$	Specific heat ratio
$K$	Eddy diffusivity
$\mu$	Dynamic viscosity

## SYMBOLS - Continued

### Greek Symbols

$\nu$	Kinematic viscosity
$\rho$	Density
$\tau$	Wall shear stress
$\Omega$	Angular velocity

### Subscripts

$( \quad )_i$	$i = 1, 2, 3$ refer to longitudinal, lateral, and vertical vector components
$( \quad )_o$	Reference value
$( \quad )_w$	Wall value
$( \underline{\quad} )$	Vector

### Superscripts

$( \quad )'$	Dimensionless with respect to some scaling parameter
$( \overline{\quad} )$	Time averaged

## TABLE OF CONTENTS

Chapter	Page
Abstract . . . . .	i
List of Tables . . . . .	ii
List of Figures . . . . .	iii
List of Symbols . . . . .	vi
1. INTRODUCTION . . . . .	1
2. GENERAL SIMILARITY CONSIDERATIONS . . . . .	4
3. SCALE CHARACTERISTICS OF METEOROLOGICAL WIND-TUNNEL FLOWS . . . . .	15
4. SIMILITUDE OF MEAN-FLOW CHARACTERISTICS FOR SMALL SCALE ATMOSPHERIC MOTIONS . . . . .	19
4.1. Modeling of the Neutral Boundary Layer . . . . .	19
4.2. Modeling of the Stratified Boundary Layer . . . . .	24
5. SIMILITUDE OF MEAN FLOW CHARACTERISTICS FOR MESO-SCALE ATMOSPHERIC MOTIONS . . . . .	31
5.1. Motion Over Topographical Surfaces . . . . .	31
5.2. Meso-Scale Atmospheric Motions . . . . .	38
5.3. Simulation of Mountain Lee-Waves . . . . .	38
5.3.1. Modeling of Mountain Lee-Waves . . . . .	39
5.3.2. Influence of Viscosity and Thermal Conductivity . . . . .	47

TABLE OF CONTENTS - Continued

<u>Chapter</u>		<u>Page</u>
6.	SIMILITUDE OF TURBULENCE FOR MICRO-SCALE ATMOSPHERIC MOTIONS . . . . .	52
6.1.	Small-Scale Turbulence (neutral thermal conditions) . . . . .	52
6.2.	Large-Scale Turbulence (neutral thermal conditions) . . . . .	56
6.3.	Small-Scale Turbulence (stable and unstable conditions) . . . . .	57
7.	SIMILARITY CRITERIA FOR TURBULENT DIFFUSION . . . . .	59
7.1.	Small-Scale Diffusion . . . . .	61
7.2.	Meso-Scale Diffusion . . . . .	66

# SIMULATION OF ATMOSPHERIC MOTION BY WIND-TUNNEL FLOWS

## 1. INTRODUCTION

Atmospheric phenomena considered for simulation in this paper are limited to mean-wind distribution, temperature distribution, turbulence, and turbulent diffusion in the lower 1000 m of the atmosphere. This is not meant to imply that wind tunnels may not be used for simulation of other atmospheric phenomena such as water-drop and hail-stone formation and growth and other aspects of cloud physics-- vertical-flow wind tunnels in laboratories at Obninsk, USSR and Davos, Switzerland have been constructed for such studies. Low-density wind tunnels have also been constructed for the purpose of studying local flow characteristics in rarefied atmosphere. Therefore, restriction to the atmospheric phenomena stated is a choice determined by interests of the staff and capabilities of the wind tunnels associated with the Fluid Dynamics and Diffusion Laboratory at Colorado State University.

The question of how well atmospheric-surface-layer flows may be simulated in the laboratory is of vital significance from both an applied and a theoretical point of view. A well-established

capability for modeling mean-flow and turbulence characteristics is of importance in many civilian as well as military applications. Within the lower 1000 m of the atmosphere urban complexes and topographic features profoundly affect the "wind" and hence air-pollution potentials, chemical and biological warfare tactics, communication by micro-wave systems, dispersion of unguided missiles, forces on stationary structures and aircraft, agricultural efficiencies, and the comfort of man and animals. In many regions the geometrical and thermal complexities are such that laboratory modeling offers the only hope for obtaining sufficient information to deal intelligently with the wind-controlled features of varied activities near the surface of the earth. Furthermore, control of air flow, geometric boundary conditions and thermal boundary conditions in the laboratory permit creation of systematically varied flows. In such flows fundamental studies can be made of turbulence structure, three-dimensional boundary layers, flow separation, and thermal and roughness effects which are useful in checking existing theoretical flow models and in developing new theoretical models.

Only by a constant effort to compare actual field data with laboratory data can there be established a reliable basis for determining the degree of simulation achieved for a particular model. Once this basis is firmly established, the necessary criteria for modeling unknown or new flow conditions to obtain specific flow characteristics

to a satisfactory degree of accuracy can be stated. When this state of knowledge is reached, the need for expensive field studies will be minimized as will be the time required to obtain pertinent design or operational data.

As in the art of modeling hydraulic structures and rivers, very seldom will it be possible to faithfully simulate all aspects of a particular flow system in the laboratory. However, this incompleteness of the hydraulic model has not detracted greatly from its practical usefulness. In attempting to simulate the atmospheric surface layer the same willingness to compromise with complete similitude must exist. However, the compromise must not be made blindly but with some knowledge of the magnitude of error introduced into the system. The primary purpose of this paper is to develop such a capability, to the extent possible with existing field and laboratory experience, by indicating the dominate scaling parameters for mean flow and for turbulence structures on scales which may vary from the micro- to the meso-range. Suggestions for the studies needed to complete this framework will be made in areas where such knowledge is deficient.

## 2. GENERAL SIMILARITY CONSIDERATIONS

For complete flow similarity in two systems of different length scales, geometrical, dynamical, and thermal similarity must be achieved. Geometrical similarity is a requirement easily realized by using undistorted scale models of the prototype geometry. On the other hand, strict dynamical and thermal similarity as required by identity of the equations of motion and energy for the two systems can be achieved only in rare cases. Therefore, at the outset one must be prepared to relax the requirement for complete dynamical and thermal similarity and attempt to achieve the best approximation. Some approximations of a general nature are discussed in the following paragraphs.

Including the major forces encountered in the atmosphere, the equations of motion in a reference system rotating with angular velocity  $\Omega$  may be written in the following form for laminar flow:

$$\frac{\partial \underline{U}}{\partial t} + \underline{U} \cdot \nabla \underline{U} + 2 \underline{\Omega} \times \underline{U} + \underline{\Omega} \times (\underline{\Omega} \times \underline{r}) = -\frac{1}{\rho} \nabla P - \frac{\Delta \gamma}{\gamma} \underline{g} + \nu \nabla^2 \underline{U} \quad (2-1)$$

The dependent and independent variables may be expressed in dimensionless form using the following scaling quantities:

$$\Omega'_i = \frac{\Omega_i}{\Omega_o}, \quad \underline{U}'_i = \frac{\underline{U}_i}{V}, \quad P' = \frac{P}{\rho_o V^2}, \quad t' = \frac{tV}{L}, \quad \underline{x}'_i = \frac{\underline{x}}{L}, \quad \underline{g}'_i = \frac{\underline{g}_i}{g_o}, \quad \rho' = \frac{\rho}{\rho_o}$$

Accordingly, a dimensionless expression convenient for inspectional analysis of the system is found to be the following:

$$\frac{V^2}{L} \left[ \frac{\partial \underline{U}'}{\partial t'} + \underline{U}' \cdot \nabla' \underline{U}' \right] + \Omega_o V (2 \underline{\Omega}' \times \underline{U}') + \Omega_o^2 L \left[ \underline{\Omega}' \times (\underline{\Omega}' \times \underline{r}') \right] =$$

$$- \frac{V^2}{L} \left( \frac{1}{\rho'} \nabla' P' \right) \frac{\Delta \gamma_o}{\gamma_o} \frac{\Delta \gamma'}{\gamma'} g_o (\underline{g}') + \frac{V \nu}{L^2} (\nabla'^2 \underline{U}')$$

or multiplying by  $L/V^2$ :

$$\frac{\partial \underline{U}}{\partial t'} + \underline{U}' \cdot \nabla' \underline{U}' + (2 \underline{\Omega}' \times \underline{U}') \frac{1}{Ro} + \left[ \underline{\Omega}' \times (\underline{\Omega}' \times \underline{r}') \right] =$$

$$- \frac{1}{\rho'} \nabla' P' - \frac{1}{Fr^2} \underline{g}' \frac{\Delta \gamma'}{\gamma'} + \frac{1}{Re} \nabla'^2 \underline{U}' \quad (2-2)$$

where

$$Ro = \frac{V}{L \Omega_o}, \quad Re = \frac{VL}{\nu}, \quad \text{and} \quad Fr^2 = \frac{V^2}{g_o L (\Delta \gamma_o / \gamma_o)}.$$

For complete dynamic similarity the dimensionless parameters  $Ro$ ,  $Re$ , and  $Fr$  (Rossby, Reynolds, and Froude numbers, respectively) would have to be the same for both the model and the prototype.

The Rossby number  $Ro$  in Eq. 2 is formed by the ratio

$$Ro = \frac{V^2/L}{\Omega_o V}.$$

Accordingly  $Ro$  may be interpreted as a ratio of inertial forces for unit mass--a reference inertial force due to rotation of the system (Coriolis' force) divided into a reference

inertial force due either to unsteadiness or nonuniformity of the velocity field. When this ratio is large rotational effects on the flow system are small compared to effects of unsteadiness or nonuniformity of the flow field. The Reynolds number  $Re$  is formed by the ratio:

$$Re = \frac{\rho V^2/L}{\mu (V/L) 1/L} .$$

It may also be interpreted as a ratio of forces

for unit mass. In this case the ratio is that of a reference inertial force divided by a reference viscous shear force. When  $Re$  is large

the inertial forces are large relative to the viscous forces. The

Froude number  $Fr^2$  is defined by the ratio  $\frac{V^2/L}{g_o \frac{\Delta \gamma_o}{\gamma_o}}$ . Thus,  $Fr^2$

is the ratio of a reference inertial force divided by a reference body force produced by differences in specific weight. A large value of  $Fr$  implies that inertial forces are large relative to the forces produced by differences in specific weight. In meteorological applications for small vertical distances, the specific weight differences arise primarily from temperature differences so that we may express  $\frac{\Delta \gamma}{\gamma_o}$  as

$-\frac{\Delta T}{T_o}$  for such flows. Thus,  $Fr^2 = \frac{-(V/L)^2}{\frac{g_o}{T_o} (\frac{\Delta T}{L})}$ , which is clearly

related to a parameter commonly known as the Richardson number

$$Ri = \frac{g_o}{T_o} \frac{\Delta TL}{V^2}$$

when written in bulk form or across a layer of finite thickness.

The Rossby number  $Ro$  can in general be eliminated from the requirements for similarity if the typical prototype length  $L$  in the horizontal plane is less than 150 km. In such cases, the Rossby number is of order  $10^{-1}$ ; and convective or local accelerations are found to dominate the Coriolis acceleration; hence, the approximation introduced by a wind-tunnel Rossby number of order  $10^{+4}$  (unless the wind tunnel were subjected to a rotation in addition to that of the earth) does not produce large differences in flow patterns between model and prototype. Therefore, the error introduced by unequal Rossby numbers is small if flow over distances less than 150 km is being simulated. This conclusion is valid also for turbulent flow.

The Reynolds number  $Re$  imposes a strong limitation on model similitude for any laminar prototype flows since the model Reynolds number will be of order  $10^{-3}$  to  $10^{-4}$  that for the prototype. This would mean that viscous forces in the model flow are more dominant than in the corresponding prototype flow. However, turbulent prototype flows--the prototype flow regime of paramount practical significance--offer greater possibilities for Reynolds-number similarity as will be discussed in a later section.

Froude-number equality or near equality can be achieved in the model and the prototype. However, special provisions for creating density stratification--heating or cooling of the wind-tunnel floor

or ceiling--must be made. Furthermore, thermal similitude as governed by the energy equation is necessary; at least in an approximate sense, if the Froude number is to be an adequate expression of the internal density stratification. An appropriate form of the conservation of thermal energy for a nonturbulent fluid is

$$\frac{\partial (C_v \rho T)}{\partial t} + \frac{\partial (C_v \rho T U_j)}{\partial x_j} + \frac{\partial (-k \partial T / \partial x_j)}{\partial x_j} = \left[ -P \delta_{ij} + \mu \left( \frac{\partial U_i}{\partial x_j} + \frac{\partial U_j}{\partial x_i} \right) - \frac{2}{3} \mu \frac{\partial U_k}{\partial x_k} \right] \frac{\partial U_i}{\partial x_j} \quad (2-3)$$

Neglecting contributions or losses of energy by processes described by terms in the bracket; i. e., pressure work, dissipation, and expansion work, and introducing the non-dimensional variables

$$t' = \frac{tL}{V}, \quad x'_j = \frac{x_j}{L}, \quad U'_j = \frac{U_j}{V}, \quad C_v' = \frac{C_v}{(C_v)_0}, \quad \rho' = \frac{\rho}{\rho_0},$$

$$k' = \frac{k}{k_0}, \quad T' = \frac{T}{\Delta T}$$

gives the following approximate non-dimensional statement for conservation of energy:

$$\frac{\partial (C_v' \rho' T')}{\partial t'} + \frac{\partial (C_v' \rho' T' U'_j)}{\partial x'_j} - \gamma \frac{1}{Pr} \frac{1}{Re} \frac{\partial}{\partial x'_j} \left( k' \frac{\partial T'}{\partial x'_j} \right) \doteq 0 \quad (2-4)$$

Here  $Pr = \frac{k}{C_p \mu}$  is the Prandtl number,  $\gamma = \frac{C_p}{C_v}$  is the ratio of specific heat at constant pressure and at constant volume. Thus, if convection of thermal energy and conduction of thermal energy dominate the thermal energy transfer the Prandtl number and  $\gamma$  should be equal for the model and the prototype. This presents no difficulty if air is the fluid in both instances.

Modeling of turbulent atmospheric-surface-layer flows is of greatest practical interest; therefore, the equations of motion should be written for this flow regime and similarity criteria sought by using the inspectional analysis technique. A useful form for our discussion is

$$\begin{aligned} \underline{\bar{U}} \cdot \underline{\bar{U}} + 2 \underline{\bar{\Omega}} \times \underline{\bar{U}} + \underline{\bar{\Omega}} \times (\underline{\bar{\Omega}} \times \underline{\bar{r}}) = -\frac{1}{\bar{p}} \nabla \bar{P} - \frac{\Delta \bar{\gamma}}{\bar{\gamma}_0} \underline{\bar{g}} + \\ \nu \nabla^2 \underline{\bar{U}} - \bar{\gamma} \cdot \nabla \underline{\bar{u}\bar{u}} \end{aligned} \quad (2-5)$$

Introducing a constant eddy diffusivity  $K$ , so that

$-\nabla \cdot \underline{\bar{u}\bar{u}} = K \nabla^2 \underline{\bar{U}}$  for convenience of estimating relative orders of magnitude, the following equation results:

$$\begin{aligned} \underline{\bar{U}} \cdot \nabla \underline{\bar{U}} + 2 \underline{\bar{\Omega}} \times \underline{\bar{U}} + \underline{\bar{\Omega}} \times (\underline{\bar{\Omega}} \times \underline{\bar{r}}) = -\frac{1}{\bar{p}} \nabla \bar{P} - \frac{\Delta \bar{\gamma}}{\bar{\gamma}} \underline{\bar{g}} + \\ \nu \nabla^2 \underline{\bar{U}} + K \nabla^2 \underline{\bar{U}} \end{aligned} \quad (2-6)$$

The corresponding non-dimensional form is, upon discarding terms

involving the Rossby number, the following:

$$\bar{\underline{U}}' \cdot \nabla' \bar{\underline{U}}' = -\frac{1}{\rho'} \nabla' \bar{P}' - \frac{1}{Fr^2} \frac{\Delta \gamma'}{\gamma'} \underline{g}' + \frac{1}{Re} \nabla'^2 \bar{\underline{U}}' + \frac{1}{(Re)_t} \nabla'^2 \bar{\underline{U}}' \quad (2-7)$$

where  $(Re)_t = \frac{VL}{K}$  is a turbulent Reynolds number. Since  $\frac{K}{\nu}$  is of order  $10^3$  we note that for turbulent flow the effective Reynolds number is about  $10^{-3}$  times smaller than for a laminar flow. This opens the possibility of achieving similarity for the gross mean characteristics of turbulent natural flows over topographical features by a laminar laboratory flow--when the scale ratio  $\frac{L_p}{L_m} = 10^3$ ,  $(Re)_m = (Re)_p$ . This type of similarity was applied by M.. Abe<sup>1</sup> in wind-tunnel studies of flow and cloud formation over Mt. Fuji. Chopra and Hubert<sup>2</sup> analyzed Karman vortex streets in the wake of islands on the basis of this type of similarity.

On the other hand, when the flow is over sharp-edged geometry, mean flow patterns are independent of the Reynolds number if the Reynolds number exceeds a lower limit which is dependent upon the geometrical form. In such instances a value of  $10^3$  for the ratio  $(Re)_p/(Re)_m$  may not introduce significant error in the modeled mean-flow patterns. However, considerable caution must be exercised in comparing turbulence statistics in such a model with prototype turbulence. The model study of winds around the Rock of Gibraltar<sup>3</sup> and the wind-tunnel model study of winds at Candlestick Ball Park<sup>4</sup> are examples of this type of modeling.

The consideration of similarity in the turbulence structure may begin with the equation for balance of turbulent kinetic energy per unit mass:  $e = \frac{1}{2} (\overline{U_i U_i}) = \frac{1}{2} (\overline{U_1^2} + \overline{U_2^2} + \overline{U_3^2})$ . When the turbulence field is steady and the only effect of the temperature field is to produce a neutral buoyancy force, the following equation-- Lumley and Panofsky<sup>5</sup> (p. 69) or Townsend<sup>6</sup> (p. 26)--expresses this balance.

$$\begin{aligned} \overline{U}_\ell \frac{\partial e}{\partial x_\ell} = & -2 \overline{u_i u_\ell} \frac{\partial \overline{U}_i}{\partial x_\ell} - 2 \frac{\partial \overline{eu}_\ell}{\partial x_\ell} - 2 \frac{\partial \overline{\rho u}_\ell}{\partial x_\ell} - 2 \nu \overline{\left( \frac{\partial u_i}{\partial x_j} \right)^2} \\ & + \frac{g}{T_0} \overline{u_i \theta} \delta_{i3} \end{aligned} \quad (2-8)$$

When attention is confined to a region near the solid boundary (0-10 m in the atmosphere or the lower  $\frac{1}{10}$  th of the boundary-layer thickness excluding the viscous wall layer near smooth boundaries, in laboratory flows) a near equality is found between energy transfer from the mean flow and energy dissipation; i. e. ,

$$2 \overline{u_1 u_3} \frac{\partial \overline{U}_1}{\partial x_3} \doteq - 2 \nu \overline{\left( \frac{\partial u_i}{\partial x_j} \right)^2} \quad (2-9)$$

In dimensionless form this becomes

$$\overline{u'_1 u'_3} \frac{\partial \overline{U}'_1}{\partial x'_3} \doteq \frac{1}{\text{Re}} \overline{\left( \frac{\partial u'_i}{\partial x'_j} \right)^2} \quad (2-10)$$

where the Reynolds number is taken to have the significant form

$$\text{Re} = \frac{Vx_3}{\nu}$$

At higher elevations in a plane homogeneous flow the dominate terms of the turbulent energy equation appear to be work done by buoyancy forces, turbulent transport of turbulent energy and dissipation or

$$\frac{g}{T_0} \overline{u_3 \theta} - 2 \frac{\partial \overline{e u_3}}{\partial x_3} - 2 \nu \overline{\left( \frac{\partial u_i}{\partial x_j} \right)^2} = 0 \quad (2-11)$$

In dimensionless form, the appropriate equation is

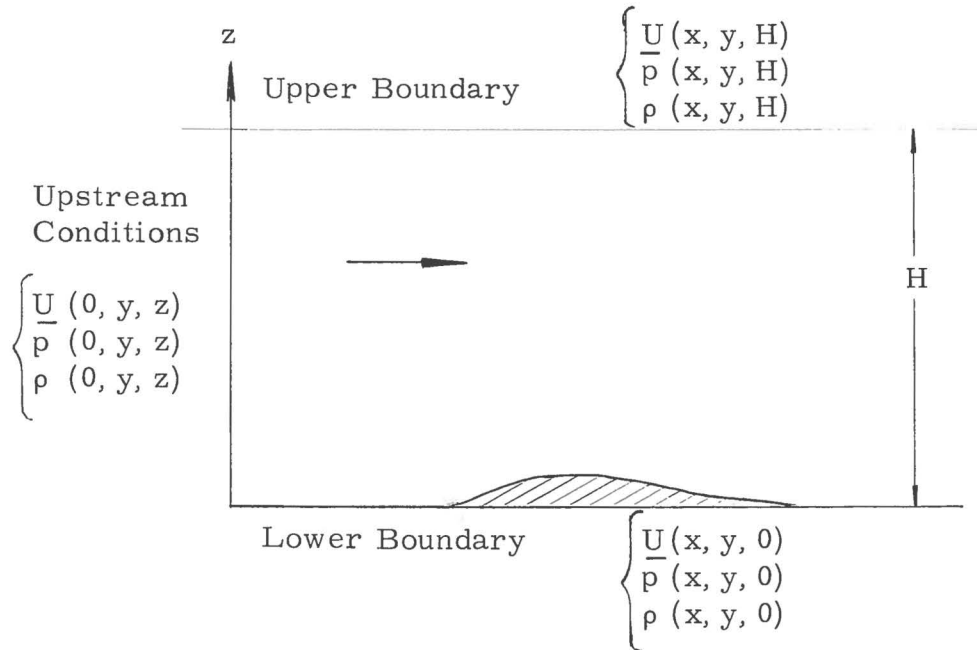
$$\text{Ri} \overline{u'_3 \theta'} - 2 \frac{\partial \overline{e' u'_3}}{\partial x'_3} - \frac{2}{\text{Re}} \overline{\left( \frac{\partial u'_i}{\partial x'_j} \right)^2} = 0 \quad (2-12)$$

where

$$\text{Ri} = \frac{g}{T_0} \frac{\Delta T (L)}{V^2} \quad \text{and} \quad \text{Re} = \frac{VL}{\nu}$$

In this case the reference length  $L$  is probably most significant when taken as the boundary distance  $x_3$ .

For complete similarity not only must the various dimensionless parameters be the same for both model and prototype, but, in addition, the boundary conditions must be the same. This latter requirement not only demands geometric similarity of the lower boundary--which is easily realized--but also similarity in upstream conditions and in conditions at the upper boundary.



The upstream conditions may be matched rather precisely by setting the model at varying distances from the leading edge of the boundary layer in the wind-tunnel test section. The velocity and density distributions that may be obtained in the tunnel are, however, all similar to one another. The upper boundary conditions can only be matched if the study of the prototype is restricted to the lower layers of the atmosphere, say about half the height of the troposphere, primarily because the increase in stability  $\frac{d}{dx_3} (\ln \rho)$  cannot be reproduced in the present wind tunnel, for this would require a sudden increase in the temperature gradient. Further development of laboratory facilities, for example superposition of thermal gradient by heated grids across the test section entrance, is needed to give more versatility in this type of modeling.

To completely simulate prototype boundary conditions the distribution of temperature over the lower boundary must be similar in both flows, and, finally, the pressure gradient  $\frac{\partial \bar{P}}{\partial x}$  must be adjusted to essentially zero in the wind tunnel.

### 3. SCALE CHARACTERISTICS OF METEOROLOGICAL WIND-TUNNEL FLOWS

The Fluid Dynamics and Diffusion Laboratory at Colorado State University currently contains two wind tunnels suitable for meteorological research. The first is a large micrometeorological wind tunnel constructed by Colorado State University for the U.S. Army under Contract DA-36-039-SC-80371<sup>7</sup>. This tunnel features a test section of 27 m length and a nominal cross-sectional area of 1.8 m by 1.8 m which can be adjusted for establishing negative and positive pressure gradients. A large contraction ratio of 9:1 in conjunction with a set of 4 damping screens yields an ambient turbulence level of about 0.1% .

The tunnel can be used for either closed or open loop operation. Test-section air velocities range from about 0 to 37 mps and the ambient temperature of the air can be varied from 0<sup>0</sup> C to 85<sup>0</sup> C at medium speeds. The humidity of the ambient air can be controlled.

The tunnel has a 12.2 m section of the test-section floor which can be heated or cooled to permit temperature differences between the cold plate and hot air of 65<sup>0</sup> C and the hot plate and cold air of more than 105<sup>0</sup> C.

A carriage system is available which permits remote placement of probes. Instrumentation associated with the facility consists of a complete system for sensing, analyzing and recording turbulence statistics and mean value of velocity, temperature and concentration (mean values only).

The second facility is a low-speed tunnel with a test section of 9 m length and a nominal cross-sectional area of 1.8 m by 1.8 m. This tunnel compliments the longer tunnel in that it allows the pursuit of less complex programs in an economical manner. The performance characteristics of the two tunnels are summarized in Table 1.

An idea of the range in boundary layer parameters measured in the Army Meteorological Wind Tunnel can be obtained by considering the variation of the classical descriptors for a specific velocity under different wall boundary conditions. For flows with neutral stability conditions (i. e. no temperature gradient) Figs.(1), (2), and (3) contains typical values of boundary layer parameters measured along the center line of the wind tunnel. A smooth surface exists along the complete tunnel length for Fig. (1). For Fig. (2) a plastic, flexible roughness was placed on the surface for the first seven meters, after which the surface was smooth. For Fig. (3) a gravel surface with rocks up to approximately 2.5 cm in diameter was placed behind the flexible roughness. As was expected the roughness increases the boundary thickness to nearly three times that of the smooth case.

Characteristic	Army Meteorological Wind Tunnel	Low-Speed Wind Tunnel
1. Dimensions		
Test-Section length	27 m	9.2 m
Test-section area	3.4 m <sup>2</sup>	3.4 m <sup>2</sup>
Contraction ratio	9.1	9.1
Length of temperature controlled boundary	12 m	3.1 m
2. Wind-tunnel drive		
Total power	200 kw	75 hp
Type of drive	4-blade propeller	16-blade axial fan
Speed control: coarse	Ward-Leonard DC control	single-speed induction motor
Speed control: fine	pitch control	pitch control
3. Temperatures		
Ambient air temperature	5 <sup>0</sup> C to 95 <sup>0</sup> C	not controlled
Temp. of controlled boundary	5 <sup>0</sup> C to 205 <sup>0</sup> C	ambient to 95 <sup>0</sup> C
4. Velocities		
Mean velocities	approx. 0 mps to 37 mps	approx. 1 mps to 27 mps
Boundary layers	up to 50 cm	up to 20 cm
Turbulence level	low (about 0.1 percent)	low (about 0.5 percent)
5. Pressures	adjustable gradients	not controlled
6. Humidity	controlled from approx. 20% to 80 % relative humidity under average ambient conditions.	not controlled

TABLE 1. Performance Characteristics of the Meteorological and Low-Speed Wind Tunnels

Figures (4) and (5) display the large-scale sizes of the average turbulent eddies measured in the wind-tunnel boundary for a neutral flow.

Flows for stable and unstable boundary conditions will vary appreciably from those of the neutral case. Figure (6) displays the variation of velocity and thermal boundary layer thicknesses for the constant temperature wall case. The details of the turbulent structure in such flows are currently being studied. The distribution of the Richardson number under several conditions are displayed in Fig. (7) and Fig. (8).

#### 4. SIMILITUDE OF MEAN-FLOW CHARACTERISTICS FOR SMALL SCALE ATMOSPHERIC MOTIONS

The wind tunnel is a research tool which has proved its usefulness for aerodynamic research on countless occasions. In meteorology, however, the wind tunnel has often been disregarded as a fluid-flow analog because of the difficulties in modeling Coriolis effects and temperature stratifications. However, if turbulent shear flows near the earth's surface are considered, then the Coriolis effect is not important, and under many circumstances the stratification of the air flow is of no consequence; hence even conventional wind-tunnel installations might find their place as useful "analog computers" for micrometeorological studies. For a large number of meteorological cases, the effect of stratification cannot be ignored; in these cases it is usually necessary to employ wind-tunnel installations specifically designed to reproduce magnitudes of stability and stratification as found in the atmosphere.

##### 4.1. Modeling of the Neutral Boundary Layer

As is well known, boundary layers in the wind tunnel are modeled by using the boundary-layer thickness  $\delta$  as the length scale, and the velocity  $V_a$  in the wind tunnel outside of the boundary layer as the reference velocity. Unfortunately, these two parameters do

not have a well defined counter part in the atmosphere. However, another set of parameters used in aerodynamics can be used to describe wind profiles in the atmospheric boundary layer. These parameters are the shear velocity  $u^*$  and roughness height  $z_0$ . The shear velocity  $u^*$  is obtained from the wall shear stress  $\tau_0$  through the relation  $u^* = (\tau_0/\rho)^{1/2}$ , where  $\rho$  is the density of the air. In the field, the parameters  $u^*$  and  $z_0$  are determined from a measured velocity profile by assuming the profile to be described by the logarithmic law of Prandtl:

$$\frac{\bar{U}_1}{u^*} = \frac{1}{k} \ln \frac{z}{z_0} \quad (4-1)$$

where  $k$  is the "universal" constant of Karman, which is generally assumed to be about 0.4. From Eq. (4-1),  $z_0$  and  $u^*$  can be determined if the wind velocities  $\bar{U}_1$  at two different elevations  $z$  are known. Values of  $z_0$  obtained in this manner have been tabulated by meteorologists for different field conditions. (See Ref. 8).

Equation (4-1) is based on results obtained for the flow along a flat plate in the wind tunnel. Clearly, for the case of a flat plate with zero pressure gradient, velocity profiles are scaled by Eq. (4-1) if  $z_0$  is used to scale the length, and if  $u^*$  is used to scale the velocity.

The value of  $z_0$  is well defined in the wind tunnel through the use of the equivalent sand roughness (Ref. 9). Therefore, a given  $z_0$  of the natural conditions can be scaled down to an equivalent sand roughness in the wind tunnel. Difficulties will, however, arise if a sand roughness is not suitable to represent the boundary of the atmospheric situation, but in general it is a simple matter of arranging, by trial and error, model roughness elements to define a usable surface.

It is not difficult to obtain a suitable shear velocity  $u^*$ .

Since the shear velocity can be written

$$u^* = \bar{U}_1 (1/2 c_f)^{1/2},$$

where  $c_f$  is the local friction coefficient, it becomes possible to establish a desired  $u^*$  by either varying the mean velocity  $U_a$  or the friction coefficient  $c_f$ . For a given mean velocity  $U_a$ , the friction coefficient depends only on the distance from the wind-tunnel entrance, or on the boundary-layer thickness,  $\delta$ , and on the viscosity,  $\nu$ , of the air. Changes of  $c_f$  with  $\delta$  and with  $\nu$  are small, however, and the most effective modeling is obtained by adjusting the mean velocity, provided that  $c_f$  for the model and for the natural situation are about of the same magnitude. Only in rare cases will it be necessary to improve the relationship by artificially thickening the boundary layer.

Both  $u^*$  and  $z_o$  are parameters depending on local conditions. If they change rapidly along the boundary then the local velocity profile cannot be expected to scale according to Eq. (4-1) even if the parameters  $u^*$  and  $z_o$  are known. The velocity distribution will reflect an average effect of local values of  $u^*$  and  $z_o$  over some area upwind of the point considered, which will increase for velocities at increasing distances from the ground.

In the meteorological wind tunnel at the Colorado State University Fluid Dynamics and Diffusion Laboratory a typical program of study of the atmospheric boundary layer has involved modeling the flow above tall crops (Ref. 10). The closest approximation to uniform boundary conditions over the region considered is probably found in and above man planted crops, where the uniformity of plant density and plant growth rate assures a reasonably uniform surface configuration.

Meteorologists since Rossby and Montgomery (1935) have used a modified logarithmic law to describe the mean velocity distributions over large crops,

$$\frac{\bar{U}_1}{u^*} = \frac{1}{k} \ln \left( \frac{z-d}{z_o} \right) \quad (4-2)$$

where  $d$  is an experimental translation distance for the vertical co-ordinate. Plate and Quraishi (Ref. 10) successfully reproduced this flow in a scaled system in the wind tunnel using arrays of flexible

plastic strips and wooden pegs to simulate the crop geometry and roughness characteristics. They were able to closely fit wind-tunnel data for non-dimensional velocity profiles above the model crops to Eq. (4-2), (see Fig. 9), and to find remarkable correspondence to field data for wind profiles within the model canopy, (see Fig. 10).

A study by Plate and Lin (Ref. 11) of the velocity field over a two-dimensional model hill indicates that there do exist model laws which permit scaling of natural boundary-layer flows which are non-uniform due to obstructions in a wind-tunnel environment. No conclusions can be drawn as yet, however, for the important flow in the standing eddy regions directly downstream of a given model.

The authors concluded that, for two-dimensional obstructions, modeling of atmospheric flows can be achieved under the conditions that:

- a. The velocity distribution in the undisturbed boundary layer be similar for model and prototype. This condition is easily met in practical cases, since the wall law, Eq. (4-1) holds both in the wind tunnel and in nature.
- b. The drag coefficient of the model hill is the same as that of the natural obstacle. A wide range of drag coefficients can be obtained by varying the stream-lining of the model hill.
- c. The ratio  $h/z_0$  must be the same for both wind tunnel and prototype.

d. The contribution of the drag integral term in the momentum equation must be the same for model and prototype. For rough boundaries where  $c_f$  is essentially a constant this implies that the horizontal scale should be given by

$$\frac{(c_f)_m}{\delta_{om}} (x_m) = \frac{(c_f)_p}{\delta_{op}} (x_p) \quad (4-3)$$

When  $(c_f)_m = (c_f)_p$  then the horizontal scale is the same as the vertical scale.

e. The disturbed velocity profiles downstream from the obstruction are similar for both model and prototype, with the same scaling parameters for the distributions as for the undisturbed velocity distribution.

f. The momentum equation with boundary-layer restrictions must be valid. This will only be true for distances downstream of the model position that ground shear is zero. This distance appears to be of the order of  $30 \cdot h$ .

#### 4.2. Modeling of the Stratified Boundary Layer

The mean velocity distribution in a thermally stratified boundary layer has been investigated by scientists working in heat transfer and in micrometeorology. The former generally assume that the effect of thermal stratification on the velocity distribution law is negligible, i. e., that the profile for neutral stability is the same as that

for stratified flow. Micrometeorologists, on the other hand, have realized that for a sufficiently large stability number the effect of the stratification can no longer be ignored, and a number of equations have been proposed in which the thermal influence on the velocity distribution is considered. Large stability numbers (Richardson numbers) occur almost regularly in nature, while those obtained in the laboratory in conventional wind-tunnel installations are generally small. Therefore, the literature on heat transfer and the literature on thermally stratified atmospheric boundary layers have developed along different lines.

Modeling of the thermally stratified atmospheric boundary layer in a wind tunnel has been an area of continued effort in the Fluid Dynamics and Diffusion Laboratory at Colorado State University. It has been found that when the Richardson number is adjusted to correspond to values found in nature the thermal stratification will also affect the profile shape in the laboratory. Subsequent data and analysis were able to demonstrate the validity of velocity distribution laws which were developed for the atmosphere, but which had only been checked against the relatively uncertain data obtained with the fluctuating winds of natural conditions. On the basis of this investigation, it was found that the logarithmic-linear law of Monin and Obukhov (1954) is in the best agreement with the experimental data.

The Richardson number has been used in the meteorological literature for different purposes. In its original derivation by Richardson (1926) it denoted a local energy parameter signifying the influence of buoyancy in enhancing or damping turbulent motion in a thermally stratified flow. It has also been used, however, as a gross parameter which describes the state of the atmospheric layer with respect to stability. It is in this connection that the Richardson number is used as a modeling parameter, and Batchelor (1953) has shown that a Richardson number modeling is sufficient to model the thermally stratified atmospheric surface layer, under some fairly general conditions.

Micrometeorologists generally work in layers where the Richardson number assumes values large enough (of positive or negative magnitude) to make it impossible to ignore the effect of buoyancy. Therefore, wind tunnel work which is meaningful for atmospheric conditions must be conducted at Richardson numbers equivalent to those found in the atmosphere. Instead of utilizing the flux Richardson number it is usually more convenient to calculate the gradient Richardson number which is easy to measure. They are related by the ratio of  $K_h$  to  $K_m$ , the exchange coefficients for heat and momentum, respectively.

$$R_f = \frac{g}{T_o} \frac{\overline{u_3 \theta}}{u_1 u_3 (\partial \overline{U_1} / \partial z)} = \frac{K_h}{K_m} \cdot Ri = \frac{K_h}{K_m} \cdot \frac{g}{T_o} \frac{(\partial T / \partial z)}{(\partial \overline{U_1} / \partial z)^2} \quad (4-4)$$

Often the assumption is made that  $K_h/K_m = \text{constant}$ ; however, recent measurements would indicate that the ratio depends on the distance from the ground. When this elementary assumption is made it is found that the Richardson number for logarithmic distributions of temperature and velocity is a linear function of height. The height dependency of the Richardson number indicates that a different type of stability may be found for different distances from the wall. For a boundary layer which is in an equilibrium layer in its neutrally stratified state, the stable regime in which buoyancy tends to reduce turbulent energy has positive Richardson numbers above some critical value. For negative Richardson numbers, the flow becomes unstable, the buoyancy supports the turbulence for values less than a certain critical magnitude.

Batchelor (1953) has shown that near a rough boundary similarity of mean velocities in a thermally stratified flow depends on a Richardson number only. Clearly, this Richardson number cannot be a local value, but must be chosen to represent gross features of the fluid motion and of the temperature field. In micrometeorology the stability parameter is calculated from values of temperature and velocity at different elevations, and since the elevations are to be scaled, it becomes necessary to define a stability parameter, independent of elevation, which has the same value for the wind tunnel flow as the quantity based on different elevations for the atmosphere. As was

mentioned previously, the conventional formulation of the Richardson stability parameter is a function of the distance from the wall, and thus, cannot be used to describe the flow field everywhere.

A constant parameter which describes the thermal stratification effects across the entire surface layer is the length  $L$  introduced by Monin and Obukhov (1954), which is defined by:

$$L = - \frac{u^{*3} C_p \bar{T}}{g k H} \quad (4-5)$$

The length  $L$  is based on the absolute average temperature  $\bar{T}$ , and on the average heat flux  $H$ . It is readily seen that this quantity assumes the significance of a scaling parameter if there exists a possibility to uniquely define both the average temperature  $\bar{T}$  and the average heat flux. Plate and Lin (Ref. 11) derived a formulation for the quantity  $L$  which depends only on the gross parameters of the wind tunnel conditions; it has the form:

$$L = - \frac{u^* U_a}{2 k g} \frac{(T_w + T_a)}{(T_o - T_a)} \left( \frac{\delta_T}{\delta} \right)^{1/m} \quad (4-6)$$

where  $\delta_T$  and  $\delta$  are the thermal and velocity boundary-layer thicknesses, respectively; and  $m$  is the integer in a power-law description of the temperature and velocity profiles. The Monin-Obukhov stability length  $L$  is frequently used by meteorologists to characterize the condition of thermal stratification in the atmospheric boundary

layer. Equation (4-6) above provides a convenient method to scale a given stability situation to wind-tunnel flows.

The logarithmic linear law was devised by Monin and Obukhov (1954) to describe the mean velocity variation of atmospheric wind profiles under various conditions of stratification. It may be written as:

$$\bar{U}_1 = u^* \left( \ln \frac{z}{z_0} + \alpha \frac{z}{L} \right) \quad (4-7)$$

where  $\alpha$  is an empirical constant and the other parameters have their usual meaning. Empirical results for the value of  $\alpha$  from meteorological data are available. Most recent investigations resulted in values of  $\alpha$  between 1 and 6 for unstable conditions (Panofsky and Lumley, 1964), and in a value of  $\alpha \approx 7$  (McVehil, 1964) for stable conditions. For the data of a study of thermally stratified flow in the wind-tunnel of the Fluid Dynamics and Diffusion Laboratory at Colorado State University a value of  $\alpha = 7$  was found to best represent stably stratified air flow. For unstable air flow,  $\alpha = 2$  appeared to be satisfactory. The agreement of the wind-tunnel data with the logarithmic-linear law is documented in Figs. (11, 12, and 13).

The assumptions used by Monin and Obukhov to develop the logarithmic linear law, Eq. (4-7) require that the shear stress and heat flux through the similarity region remain constant. In wind tunnel flows these requirements are only approximated in regions

close to the wall; hence, rates of turbulent diffusion and velocity profiles implied by the similarity theory should not be utilized for  $z/\delta > 0.4$ .<sup>(12)</sup> The velocity profiles in the outer nine-tenths of the neutral boundary in the Army Meteorological Wind Tunnel have been noted to consistently agree with velocity-defect relations such as that derived by Coles<sup>9</sup>.

The various modeling criteria outlined in the preceding paragraphs have been applied to studies carried out in the Fluid Dynamics and Diffusion Laboratory at Colorado State University. These programs have included the study of wind abatement about Candlestick Ball Park, San Francisco, California<sup>4</sup>; evaporation studies of Lake Hefner, Oklahoma<sup>13</sup>; force distribution over the proposed World Trade Center, New York City<sup>14</sup>; and wind perturbations around a meteorological tower at White Sands Missile Range, New Mexico<sup>15</sup>.

Figure 14 gives a comparison of prototype and model (1:800 scale) flow pattern over Candlestick Ball Park. Generally, the mean flows are in excellent agreement.

## 5. SIMILITUDE OF MEAN FLOW CHARACTERISTICS FOR MESO-SCALE ATMOSPHERIC MOTIONS

### 5.1. Motion Over Topographical Surfaces

Generally speaking, wind problems such as are encountered in flows over large topographical features of the earth may be classified under the broad heading of "Terrain Aerodynamics". Terrain aerodynamics may be described as a study, laboratory and/or field, of the effect of local topography on the wind distribution and the contribution of the terrain to the local turbulence or gustiness. In general, of course, terrain features must be limited to prototype lengths less than 150 km if it is to be assumed that convective or local accelerations dominate the Coriolis forces in a model study.

One of the earliest scale (1:50,000) model experiments for this type of study was carried out in Japan by Abe (Ref. 1) in 1928 with a model of Mount Fujiyama. The contours of Fujiyama being quite smooth, the flow pattern was affected to a large degree by the local Reynolds number which was approximately 50,000 times smaller than in the prototype. Thus, the model flow patterns obtained were not even qualitatively close to that observed in actual field tests. On the other hand, Reynolds number effects have less influence on flow over rough, craggy terrain; therefore, true mean flow patterns can

be obtained from the wind tunnel air flow over a scale model of such terrain.

For atmospheric flows over rough sharp edged topographical features viscous effects no longer dynamically govern the flow; hence the appropriate equation of motion would take the form suggested by Euler for potential flow:

$$\underline{U} \cdot \nabla \underline{U} = \frac{1}{\rho} \nabla P - \frac{\Delta\gamma}{\gamma} \underline{g} \quad (5-1)$$

Coriolis accelerations are assumed negligible and are eliminated above. The dependent and independent variables may be expressed in dimensionless form using the following scaling quantities:

$$U'_i = \frac{U_i}{V}, \quad P' = \frac{P}{\Delta P}, \quad x'_i = \frac{x_i}{L}, \quad g'_i = \frac{g_i}{g_0}, \quad \gamma' = \frac{\Delta\gamma}{\gamma_0} \quad (5-2)$$

Accordingly, a dimensionless expression which emphasizes important scaling parameters is the following

$$\underline{U}' \cdot \nabla \underline{U}' = - \frac{Eu}{2} \nabla P' - \frac{1}{Fr^2} \underline{g}' \frac{\Delta\gamma'}{\gamma'} \quad (5-3)$$

where

$$Eu = \frac{\Delta P}{\rho V^2 / 2} \quad ; \quad \text{and} \quad Fr^2 = \frac{V^2}{gL(\Delta\gamma_0/\gamma_0)} \quad .$$

Hence for dynamic similarity of flows over sharp edged topographical

features the dimensionless parameters  $Eu$  and  $Fr$  (Euler and Froude numbers) would have to be the same for both the model and the prototype.

The Euler number  $Eu$  normally only requires geometric similarity between model and prototype. This assures general similarity of the gross wind directions and distributions of vortices, eddies, and vertical currents. It can not be expected that the actual strength and rapidity of fluid motions would be found on the model, however, such measurements must usually be made in the field on the prototype.

An example of a successful study of terrain aerodynamics in the laboratory was that performed in 1929 at the National Physical Laboratory of Great Britain (Ref. 3), on the 1:5000- scale model of the Rock of Gibraltar in a low-speed wind tunnel. This study was instigated in order to determine the types and distribution of possible disturbances before a full scale field study was begun.

In the model investigation two methods were used to determine the wind patterns caused by the Rock. In the first, an extensive grid of some 800 "flags", two-inch silk fibers spaced at regular lateral and vertical intervals, was fixed with the wind tunnel. These flags were observed for range and violence of movement and for prevailing wind direction in pitch and yaw. In the second method, long streamers of fine wool fibers were placed in various critical positions, and a

record of streamline patterns was made. The wind speed used was about 25 feet per second, and the wind direction was varied from northeast through east to southeast. It was found that wind directions and the distribution of vortices and vertical currents obtained with the model agreed closely with those occurring in nature at Gibraltar. In the case of features of the wind such as the actual intensity of gustiness and the rapidity of changes in direction and gustiness, the modeled flow was not in good agreement with the prototype flow.

Although the wind tunnel study was limited to providing wind from one direction and at one strength at a time over the Gibraltar model there were only 24 cases of discordance out of 360 plottings of test balloons over the prototype. When the balloons repeated each other, and their results could be averaged, the agreement was very good. Before the model work began it was predicted on theoretical grounds that large scale eddies would develop and break away from the Rock with a period of something like 3 minutes in a steady wind. An inverted half cylinder lain prone with its axis across the wind is a known case in model form; eddies form in lee of its ridge and at a given stage of development, or after a given time interval, they break off and travel down wind to make a way for their successors to form. The Rock is more bluff than a half cylinder, but the period relationship was expected to hold approximately. Field observations of cloud behavior above Gibraltar revealed a period of approximately 4-5 minutes.

Similar satisfactory results have been obtained in the Fluid Dynamics and Diffusion Laboratory at Colorado State University while modeling various terrain features. A wind tunnel study of a 1:12,000 scale model of Point Arguello area in California was made to estimate the mean flow and diffusion characteristics of toxic gases which might be released in the vicinity of missile launch sites on the U. S. Naval Missile Facility. Similarity in flow patterns between model and prototype was established for inversion flows approaching from the northwest. (See Ref. 22). This study differed from the Rock of Gibraltar study in that the flow was not dominated by the geometry. Accordingly, to obtain the best simulation of mean flows, the idea of Abe was used in which Reynolds numbers were composed on the basis of a molecular and turbulent viscosity for model and prototype respectively. Using such a comparison the flow over the Point Arguello model was essentially laminar. The study was considered to be exploratory in nature. No attempt had been made in previous studies to model wind patterns using such a small scale model with the exception of Abe's effort. For terrain modeling purposes, neither a wind tunnel capable of creating flow with a density gradient nor adequate field data for comparison of inversion flow results had been available until development of the Army meteorological wind tunnel.

Model-prototype wind-flow similarity for the Point Arguello study was assured through the following elements:

a. Geometrical similarity--a 1:12,000 scale model of Point Arguello was provided.

b. Similarity of the mean wind distribution (vertical) approaching the land mass--the log-linear velocity distribution measured in atmospheric flows was duplicated by portions of the wind tunnel boundary layer. This was accomplished in spite of the stabilizing effect of the inversion structure because of the log velocity distribution developed upstream from the chilled plate.

c. Similarity of the mean-temperature distribution (inversion) approaching the land mass--a cooled floor on the wind tunnel achieved values of the Richardson number greater than 0.25. This assured the existence of a region of stable stratification or inversion.

Comparison of wind tunnel and prototype data established at least a qualitative similarity in the structure of the temperature field over the Point Arguello area. Comparison of the surface flow directions and smoke traces for neutral and inversion flows established an excellent agreement in wind flow patterns over the Point Arguello area for flows approaching from the northwest. (Fig. 15).

A 1:6200 scale model of San Nicolas Island off the California coast line has also been studied under conditions of inversion flow in the Meteorological Wind Tunnel. (See Ref. 23). Visualization procedures, including colored indicator paints and titanium tetrachloride smoke, were used to determine characteristic flow patterns over the

island with wind orientation to the island of  $315^{\circ}$ . (Figures 16 and 17). Diffusion of toxic rocket exhaust products were simulated by the release of controlled amounts of helium. Concentration profiles of the helium plume were measured at various distances downwind of the island model. Similar flow patterns were observed from model to prototype, and pictures of eddy smoke in the lee edge of the island model duplicated eddy characteristics apparent in equivalent pictures taken over the prototype. (See Figs. 17 and 18).

From the brief review of "terrain aerodynamics" given above, it is seen that several scale model studies of the wind pattern over terrain models with scale ratios in the range of 1:5000 to 1:50,000 have been conducted in the past - most of these have been partially successful. In general, modeling of flow over "sharp" isolated topographic features has yielded satisfactory results, since, for these cases, the flow patterns are independent of Reynolds number when this number exceeds some lower limit. In such cases a turbulent atmosphere flow is simulated by a turbulent laboratory flow. When the scale ratio becomes smaller than about 1:5000 and the terrain features are not isolated but form a hill-valley complex, the flow pattern depends strongly on the Reynolds number. For these cases, a laminar laboratory flow can be used to simulate the turbulent atmospheric flow. Using a molecular Reynolds number for comparison with a turbulent viscosity Reynolds number gives a near equality at the small scales currently used because of the restrictions imposed by wind tunnel size.

## 5.2. Meso-Scale Atmospheric Motions

Recent data provided by weather satellites have revealed another example of how atmospheric phenomena may be related to fluid properties studied in the laboratory. (Ref. 2). The properties of meso-scale eddies in the wake of islands were investigated in the light of their apparent resemblance to the Karman vortex-street pattern. By use of the theoretical results from drag theory and the observed quantities such as cross-stream diameter of the obstacle, wind speed, and the dimensions of the pattern, estimates were made for the shedding of eddy pairs, the lateral and longitudinal spacing between the vortices and the lifetime of the eddies and drag on the island. These estimates for the various characteristic parameters of the eddy pattern were in good agreement with their corresponding values in the laboratory experiments where stable vortex sheets become discernible.

## 5.3. Simulation of Mountain Lee-Waves

The restoring force in the production of atmospheric gravity waves is provided by the earth's gravity, as their name indicates. But it should be stressed that the presence of gravity is not sufficient to generate waves because the restoring or buoyancy force only appears in a fluid if the latter is non-homogeneous (or stratified), for otherwise a parcel of fluid is in a state of indifferent equilibrium at any location and never tends to return to its original position.

In order to simulate atmospheric gravity waves in a wind tunnel, the modeling apparatus must possess the capability of introducing enough stratification in the air to reproduce a ratio of inertial to gravity forces - embodied in the Froude number - of the same order of magnitude as occurs in the natural atmosphere. Similarity in boundary conditions must also be satisfied.

In addition to these requirements, the problem is further complicated by the fact that in the prototype viscosity and thermal conductivity have a negligible effect whereas, on the scale of wind tunnel experiments they cannot be disregarded.

It shall first be shown that the proper conditions of stratification and velocity can be attained in the wind tunnel at Colorado State University, for if these conditions were out of reach any further considerations would be in vain. Next we shall attempt to show that under certain restrictions viscosity and thermal diffusivity do not radically affect the wave pattern in the wind tunnel.

### 5.3.1. Modeling of Mountain Lee-Waves

Governing equations - If we disregard viscosity and molecular diffusion for the time being, the energy equation reduces to the adiabatic equation.

$$U_i \frac{\partial P}{\partial x_i} = c^2 U_i \frac{\partial \rho}{\partial x_i} \quad (5-4)$$

If in addition the scale of the atmospheric motion is not large, say of the order of 1 km or less - both prototype and model flow are incompressible, the mach number  $V/C$  being without doubt very small, then

$$U_i \frac{\partial \rho}{\partial x_i} = 0 \quad (5-5)$$

In other words, the energy equation reduces to equation of incompressibility, and in this case does not introduce any similitude requirement.

The non-dimensional momentum equation for inviscid motion is (see Eq. 1-2).

$$\frac{\partial \underline{U}'}{\partial t'} + \underline{U}' \cdot \nabla \underline{U}' = - \frac{1}{\rho'} \nabla P' + \frac{1}{Fr^2} \frac{\Delta y'}{y'} \underline{g}' \quad (5-6)$$

in which the only non-dimensional parameter is the Froude number

$$Fr = \frac{V}{\sqrt{g L \frac{\Delta \rho_0}{\rho_0}}}$$

The main requirement for simulating gravity waves is therefore, to obtain a Froude number for the model  $(Fr)_M$  of the same order as the one existing in the prototype flow  $(Fr)_P$ , i. e.

$$(Fr)_M = (Fr)_P \quad (5-7)$$

$\frac{\Delta \rho_o}{\rho_o}$  is a measure of the stability or degree of stratification

of the fluid.  $\Delta \rho_o$  is the difference in density of an air parcel, which initially was at level 1 and is brought to level 2, with the new surrounding medium at level 2. Since in a normal atmosphere the lapse rate

$$\frac{\partial T}{\partial z} = -\alpha \quad (5-8)$$

is small, typically  $10^{-2}$  °C/m, the temperature change due to adiabatic heating or cooling must be taken into account because of the difference in pressure between level 1 and 2. If the amplitude of the vertical displacement is of the order of the height of the mountain  $L$ , we have then

$$\frac{\Delta \rho_o}{\rho_o} = L \frac{\alpha_a - \alpha}{T} = L \sigma \quad (5-9)$$

where

$$\alpha_a = \frac{g}{C_p}$$

is the adiabatic lapse rate. In meteorology  $\sigma$  is commonly called the stability. The Froude number can, therefore, also be written

$$Fr = \frac{V}{L} \sqrt{\frac{T}{g(\alpha_a - \alpha)}} = \frac{V}{L \sqrt{g \sigma}} \quad (5-10)$$

Perturbation equation - The governing differential equation for mountain lee-waves obtained by classical perturbation theory is (see Ref. 24 p. 51):

$$\nabla^2 w_1 + f(z) w_1 = 0 \quad (5-11)$$

where:

$$w_1 = \left( \frac{\rho}{\rho_0} \right)^{1/2} w \quad \text{is the modified vertical perturbation velocity}$$

$$f(z) = \frac{\sigma g}{\underline{U}^2} + \frac{S}{\underline{U}} \frac{d\underline{U}}{dz} - \frac{1}{4} S^2 + \frac{1}{2} \frac{dS}{dz} - \frac{1}{\underline{U}} \frac{d^2 \underline{U}}{dz^2}$$

$$\underline{U} \quad \text{is the undisturbed horizontal velocity}$$

$$S = \sigma + g/c^2$$

By making the differential equation dimensionless, we obtain

$$\nabla^2 w_1' + L^2 f(z) w_1' = 0 \quad (5-12)$$

For rigorous similarity it would be necessary for the function  $L^2 f(z)$  to be identical in the prototype and the model. But for approximate similarity it will be sufficient to match a characteristic numerical value of  $L^2 f(z)$ . The dominant term  $f(z)$  is the first one, so that

$$f(z) \simeq \frac{\sigma g}{\underline{U}^2} \quad (5-13)$$

and a characteristic value of  $L^2 f(z)$  - sometimes called the Lyru parameter in mountain lee-wave theory - is therefore

$$\frac{1}{Fr^2} = \frac{\sigma g L^2}{V^2} \quad (5-14)$$

We find thus the Froude number again.

Exact differential equation - The same result is, of course, found when the exact partial differential equation governing the air flow over a mountain is considered rather than the perturbation equation. This equation in non-dimensional form is (see Ref. 25)

$$\nabla^2 y'_0 + \frac{1}{2} \left[ (\nabla' y'_0)^2 - 1 \right] \frac{d}{dy'_0} (\ln \rho' U'^2_0) - \frac{gL}{V^2 U'^2_0 \rho'} \frac{d\rho'}{dy'_0} (y'_0 - y') = 0 \quad (5-15)$$

where  $y'_0$  is the altitude of a particle far upstream and  $y'$  its altitude at any position,  $U'_0$  is the horizontal velocity distribution far upstream. The curves  $y'_0(x, y) = \text{constant}$  are streamlines.

From this equation it can be seen that rigorous similarity requires identical velocity and density distributions upwind of the barrier and the same numerical value of the parameter  $\frac{gL}{V^2}$  in the prototype and the model. The coefficient  $\frac{d}{dy'_0} (\ln U'^2_0 \rho')$  being small in general and for moderate variations of  $U'_0$ , approximate similarity only requires the matching of the parameter:

$$\frac{gL}{V^2} \frac{1}{\rho'} \left( \frac{d\rho'}{dy'_0} \right) \simeq \frac{gL \Delta\rho/\rho}{V^2} \quad (5-16)$$

which is  $1/\text{Fr}^2$ .

Modeling requirements - The equality of the Froude numbers in the prototype (index P) and the model (index M)

$$\frac{V_P}{L_P \sqrt{g \sigma_P}} = \frac{V_M}{L_M \sqrt{g \sigma_M}} \quad (5-17)$$

yields

$$\frac{V_M}{V_P} = \frac{L_M}{L_P} \sqrt{\frac{\sigma_M}{\sigma_P}} \quad (5-18)$$

$$\begin{aligned} \text{We have } C_p &= 9.89 \times 10^2 \text{ m}^2 \text{ sec}^{-2} \text{ } ^\circ\text{C}^{-1} \\ g &= 9.89 \text{ m sec}^{-2} \end{aligned}$$

hence

$$\alpha_a = 10^{-2} \text{ } ^\circ\text{C}/\text{m}$$

For a typical stratified atmosphere  $\alpha \simeq 0.6 \times 10^{-2} \text{ } ^\circ\text{C}/\text{m}$ .

$$\text{Hence for } T = 270 \text{ } ^\circ\text{R}$$

$$\sigma_P = \frac{\alpha_a - \alpha_P}{T_P} \simeq 1.5 \times 10^{-5} \text{ m}^{-1}$$

In the wind tunnel at Colorado State University a temperature difference of about  $100^{\circ}\text{F}$  can be maintained across the air between the floor and the center of the tunnel. If the temperature boundary layer is one foot thick and the average temperature  $30^{\circ}\text{C}$ ,

$$\alpha_M \approx -\frac{100^{\circ}\text{F}}{7\text{ ft}} = -1.8 \times 10^2 \text{ }^{\circ}\text{C/m}$$

the minus sign indicates the temperature increases with increasing height, hence

$$\sigma_M = \frac{\alpha_0 - \alpha_M}{T_M} \approx 0.6 \text{ m}^{-1}$$

Thus

$$\frac{\sigma_M}{\sigma_P} = 4 \times 10^4$$

Suppose a mountain 1 km high is being modeled. If the stratified layer in the tunnel is 0.3 m thick, the model height should not exceed 1/3 of this height. Then

$$L_M = 4 \text{ in} \approx 10^{-1} \text{ m}$$

and then

$$\frac{L_M}{L_P} = 10^{-4}$$

which yields

$$\frac{V_M}{V_P} = 2 \times 10^{-2}$$

Field observations have shown that mountain lee-waves generally occur for wind speeds ranging between 7 and 20 m/sec (see Ref. 24 p. 48 and p. 55):

$$7 \text{ m/sec} < V_P < 20 \text{ m/sec} \quad (5-19)$$

This requires then that

$$14 \text{ cm/sec} < V_M < 40 \text{ cm/sec} \quad (5-20)$$

These velocities although extremely small and difficult to measure can be obtained in the wind tunnel at Colorado State University. The corresponding Froude numbers are

$$0.6 < Fr < 1.6 \quad (5-21)$$

Boundary conditions - The upstream boundary conditions for the model can approximately be matched to those of the prototype; however, since the velocity and temperature distributions are produced naturally by the boundary layer development these profiles have definite shapes which cannot easily be changed.

The lower boundary condition can easily be satisfied by constructing a model geometrically similar to the prototype.

The matching of the upper boundary conditions presents the greatest difficulty. The atmosphere, indeed, is non-homogeneous throughout and presents even a strong increase in stability from the troposphere on up. In the wind tunnel, the fluid above the stably stratified layer is homogeneous, i. e., the stability is zero. The increase in stability at the troposphere could thus only be simulated by heating the air at a certain height from the tunnel floor above the ambient temperature, a provision which does not exist in the wind tunnel at Colorado State University.

However, if the mountain lee-wave phenomena is only considered in the lower layers of the atmosphere, it can intuitively be assumed that the effect of the troposphere is small. The modeling of gravity waves should, therefore, be restricted to those generated by mountains at most a few kilometers high. Waves produced by a mountain range rising 1 km above the flatlands - a height one tenth that of the troposphere - may be satisfactorily simulated in a wind tunnel.

### 5.3.2. Influence of Viscosity and Thermal Conductivity

The scale of atmospheric motions and hence the magnitude of the Reynolds number are so large as to render the viscous and diffusive terms in the equations of motion negligible, except in a thin layer close to the ground. The scale of the model, on the contrary,

is such that these molecular effects cannot be neglected. The question, therefore, arises whether viscous and diffusion effects in the model will distort the wave pattern to an extent such that it will retain little in common with the atmospheric waves.

To answer this question rigorously, one must solve the equations of motion with identical boundary conditions for a real fluid on one hand and for a non-viscous, non-diffusive fluid on the other hand, and to compare the two solutions. This would be a formidable task owing to the prodigious complexity of the equations of motions which today have only been solved either when the buoyancy forces are negligible (forced convection) or when the driving force is solely produced by buoyancy (free convection) and this for particular boundary conditions.

In the absence of complete solutions to the problem, we may compare results of homogeneous viscous-diffusive flow and of non-homogeneous non-viscous non-diffusive flows, keeping in mind that owing to the non-linearity of the equations of motion the effects of non-homogeneity and those of viscosity-diffusivity are not simply additive. But we may compare the order of magnitudes of these effects in the model.

First, let us calculate the wave length of the mountain wave generated by the model (see Ref. 24 p. 55)

$$\lambda_M = \frac{2\pi V_M}{\sqrt{g \sigma_M}} \quad (5-22)$$

For  $\sigma_M = 0.6 \text{ m}^{-1}$  and  $V_M = 0.3 \text{ m/sec.}$

$$\lambda_M \simeq 0.75 \text{ m}$$

Next let us consider a laminar boundary layer. The thickness of the boundary layer is given by (see Ref. 9)

$$\delta = C \left(\frac{\nu}{V}\right)^{1/2} x^{1/2} \quad (5-23)$$

where  $C$  is a numerical constant ( $C \sim 5.2$ ) and  $x$  is the distance from the leading edge of the flat plate over which the boundary layer is being created. A small change in boundary-layer thickness occurs then over the distance  $\Delta x$  such that

$$\frac{\Delta \delta}{\delta} = \frac{1}{2} \frac{\Delta x}{x}$$

A change in boundary-layer thickness of 10% requires thus a distance

$$\Delta x = 2 \left(\frac{\Delta \delta}{\delta}\right) x = \frac{x}{\delta} \quad (5-24)$$

Hence the farther from the leading edge, the larger the distance required to produce a given relative increase in boundary layer thickness. Thus at a distance of 20 m ( $\sim 60$  ft) from the entrance

of the test section, which has a total length of 26 m ( $\sim 80$  ft) in the wind tunnel at Colorado State University, a boundary layer increase of 10% will require a distance  $\Delta x$  of 4 m.

This distance of 4 m corresponds to approximately 5 wave lengths as computed above. Since the Prandtl number for air is of the order of one, the temperature layer varies in similar fashion as the boundary layer.

If, therefore, the gravity waves are tested far downstream from the entrance of the test section, it may be concluded that viscosity and thermal diffusivity exert a minor influence on the wave pattern.

This results can also be arrived at by comparing the vertical velocities due to mountain waves on one hand and due to boundary layer build-up on the other hand. From continuity the latter velocity  $W_{B, L}$ , is related to the free stream velocity  $V$  by

$$C' V \Delta \delta = W \Delta x$$

where  $C'$  is a constant depending on the velocity distribution ( $C' \simeq 3/10$ ).

$$\text{Then } \frac{W_{BL}}{V} = C' \frac{\Delta \delta}{\Delta x} = \frac{C'}{2} \frac{\delta}{x} = \frac{C'}{2} \sqrt{\frac{\nu}{Vx}}$$

Since the vertical velocities  $W_{MW}$  in mountain lee-waves are of the same order of magnitude as the horizontal velocities:

$$W_{MW} \sim V$$

we have 
$$\frac{W_{BL}}{W_{MW}} \sim \frac{C'}{2} \sqrt{\frac{\nu}{Vx}}$$

Thus for air and  $x = 20 \text{ m}$ ,  $V = 0.3 \text{ m/sec}$

$$\frac{W_{BL}}{W_{MW}} \sim 2 \times 10^{-4}$$

At a distance of 20 m from the entrance of the test section and for a free stream velocity of 0.3 m/sec, which are required for the simulation of mountain lee-waves in the wind tunnel, the vertical velocity due to the increase in boundary layer thickness is at least one thousand times smaller than the vertical velocity due to the mountain waves.

It may, therefore, be concluded that far enough from the entrance of the test section, say about 20 m, the effects of viscosity and thermal diffusivity are small compared to the effect of gravity provided the velocity and density stratification are adequate.

## 6. SIMILITUDE OF TURBULENCE CHARACTERISTICS FOR MICRO-SCALE ATMOSPHERIC MOTIONS--TURBULENCE

The modeling of the turbulent structure in a surface layer appears to be divided into two parts. First, the large-scale character of the turbulence appears to be directly related to the surface-layer roughness. The small-scale character of the turbulence has been found to scale directly with the turbulent dissipation. The small scale turbulence motion will be discussed first, since it appears to be well understood. Flows with neutral thermal structures will be considered and then will be followed by a discussion of certain features of thermally stable and unstable turbulent flow.

### 6.1. Small-Scale Turbulence (neutral thermal structure)

The concept of local isotropy, first proposed by Kolmogoroff, (Ref. 27) requires that the small-scale turbulence become spherically symmetrical at sufficiently large Reynolds numbers. Local isotropy leads to the requirement that the spectral energy distribution of the small scale motion is given by the relation

$$f(k) = \frac{\epsilon^{1/4} \nu^{5/4}}{u^2} F(k/k_s) \quad (6-1)$$

where  $\nu$  is the kinematic viscosity, and  $k_s = (\epsilon \nu^{-3})^{1/4}$ . The total

dissipation of turbulent energy per unit mass is  $\epsilon$ . It now appears that  $F$  is a universal function, which may be determined from measurements. The term  $\overline{u^2} f(k)$  may be written  $\frac{U}{2\pi} \overline{u_f^2}$ , where  $U$  is the local mean velocity and  $\overline{u_f^2}$  is the mean square turbulent velocity at the frequency  $f$ . Thus, the small-scale turbulent motions,  $\overline{u_f^2}$ , can be determined once  $U$  and  $\epsilon$  are specified.

Figure 19 shows the universal nature of the function  $F$  for both atmospheric and wind-tunnel flow, as well as flow in water. Measurements in the wind tunnel indicate that  $F$  is independent of surface roughness, (Fig. 20 a, b, and c.) There is a minimum length of boundary layer development required before the turbulence becomes similar. Measurements in the Army wind tunnel appear to indicate similarity at distances greater than 8 m from the entrance. Exploration of the first 8 m of the tunnel will be made in the future.

The data available from atmospheric measurements is limited in extent, so it is difficult to establish definite numerical scales for the turbulent dissipation. Table 2 lists the value of dissipation reported by Pond, Stewart and Burling, (Ref 28), for wind over waves. The values of dissipation obtained in the wind tunnel are also listed in the table. The scaling factor  $\frac{\epsilon_{\text{wind tunnel}}}{\epsilon_{\text{atmosphere}}}$ , for the turbulent dissipation ranges from 2 to 2350. The smooth-plate, wind-tunnel case is probably the closest to the atmospheric measurements, so the scaling

TABLE 2. Magnitudes of Turbulent Dissipation for Atmospheric and Laboratory Flow Conditions

Turbulent Dissipation $\text{cm}^2/\text{sec}^3$	Flow Conditions	Height	Source
87	Atmospheric		Ref. 28
95	wind	1 m	
90	over water	above water	
80			
0.003 to 1	Ocean water	7.5 m below water surface	Ref. 30
43,200 to 186	Army wind tunnel Smooth surface	1.3 to 51 cm	Ref. 31
32,500 to 5,580	Army wind tunnel 7.5 meters Flexible roughness then smooth surface	1.3 to 51 cm	unpub.
211,000 to 1,860	Army wind tunnel 7.5 meters flexible roughness then Gravel roughness	1.3 to 51 cm	unpub.

range might be from 2 to 480 . Table 3 lists the values of  $F(k/k_s)$  versus  $k/k_s$  , which are an average of the data given in Fig. 20 a, b, and c.

TABLE 3. Average Values for Universal Spectral Energy Distribution Function Obtained from Meteorological Wind Tunnel Data

$\frac{k}{k_s}$	$F\left(\frac{k}{k_s}\right)$
$3.98 \times 10^{-3}$	$9.32 \times 10^3$
6.30 "	4.57
$1.00 \times 10^{-2}$	2.14
1.58 "	$8.90 \times 10^2$
2.51 "	4.27 "
3.98 "	1.90 "
6.31 "	$7.34 \times 10^1$
$1.00 \times 10^{-1}$	2.92 "
1.58 "	1.33 "
2.51 "	$1.85 \times 10^0$
3.98 "	$7.46 \times 10^{-1}$
6.31 "	$6.82 \times 10^{-2}$
$1.0 \times 10^0$	$7.40 \times 10^{-3}$

The scaling of the turbulent dissipation from the wind tunnel to the atmosphere will require further knowledge about both types of flow. As Table 2 shows, there is a fairly wide variation in  $\epsilon$  . Present measurements in the Army wind tunnel indicate the quantity  $\frac{\epsilon}{u^2}$  is a function of only the vertical location in the boundary layer and not of horizontal distance along a flow. Figure 21 shows values of  $\frac{\epsilon}{u^2}$

measured over three different types of surface roughness. There is a slight variation of  $\frac{\epsilon}{u^2}$  due to surface roughness, but, with the exception of the inner viscous region, the variation of  $\frac{\epsilon}{u^2}$  from the 12 m to the 22 m station is within the scatter of the measurements. For modeling purposes, it would appear that  $\frac{\epsilon}{u^2}$  could be represented by one universal curve in vertical distance.

## 6.2. Large-Scale Turbulence (neutral thermal conditions)

The large scale structure of the turbulence is by no means as well understood as the small scale. In general, it appears that the large scale structure will be closely related to the "local" surface conditions. The value  $\overline{u^2}$  should be mainly determined by the large eddies, so that the results of Fig. 21 indicate a possible interrelation between the small and large structure. The large-scale motion is usually characterized by a scale or wave length. By plotting a curve of  $f F(n) \frac{\overline{u^2}}{U^2}$  versus  $k$ , where  $F(n) = \frac{2\pi}{U} f(k)$ , a dominate wave length may be defined. Figure 22 a, b, and c is a typical plot of the smooth-surface spectra measurements in the form of  $f F(n) \frac{\overline{u^2}}{U^2}$  versus  $k$ . The peak value of  $f F(n) \frac{\overline{u^2}}{U^2}$  is assumed to correspond to a dominate wave length which is employed to characterize the large-scale turbulence. Figure 23 shows a typical curve obtained for the spectrum of atmospheric turbulence, (Ref. 29). The wave length for the average curve of Fig. 23 corresponds to a turbulent scale length of approximately 650 meters. The curves of Fig. 22 a, b, and c give scale

lengths of from 12-21 cm. This gives a range of modeling factors of from 500 to 2900 for the flows in the wind tunnel. The effect of a rough surface is to increase the tunnel scale and reduce the modeling factor. The effect of free-stream velocity is to change the scale directly with velocity.

### 6.3. Small-Scale Turbulence (stable and unstable thermal conditions)

In thermally stratified shear flow, modeling of the turbulent structure appears to depend on Richardson number  $Ri$  which is a function of the Monin-Obukhov similarity length scale  $L$ , height from the wall  $z$ , and a parameter  $\beta$  in the following way:

$$Ri = \frac{z}{L} \frac{1}{1 + \beta \frac{z}{L}} ;$$

The turbulent intensity of the vertical velocity component measured in the field as well as in the wind tunnel has been shown to be a function of Richardson number only, provided that the corresponding wall-distance Reynolds numbers are comparable. Figure 24 shows the dependence of dimensionless, turbulent intensity of the vertical velocity component, both field and wind tunnel data, upon the Richardson number. The disagreement at 150 cm/sec is a result of relatively larger viscous forces modifying the turbulence. Therefore, both a Richardson number, and Reynolds number are scale factors.

For the neutral flow with high Reynolds numbers, local isotropy can be expected to occur and the turbulent energy spectrum will have a large frequency range following the  $5/3$  power law. For the stable flow, a tendency toward the  $-11/5$  power law as suggested by Bolgiano, (Ref. 32) is seen. No isotropy was observed in the unstable and neutral flows with low Reynolds numbers. However, the turbulent energy in the lower frequency range contributes most of the turbulent energy so that Richardson number in the wind tunnel is an order of magnitude smaller than that in the field. This is proved to be the case as shown in Fig. 24, where the Reynolds number for the wind tunnel data at 300 cm/sec is about two orders of magnitude smaller than that estimated from the field data, (Ref. 33).

Experimental turbulence data from the Army wind tunnel and the atmosphere show interesting similarities, however, much effort is still necessary to establish with certainty the proper length scale or scales relating laboratory and atmospheric flows under all thermal and roughness conditions.

## 7. SIMILARITY CRITERIA FOR TURBULENT DIFFUSION

As is well known, turbulent diffusion is a phenomenon which disperses matter, heat etc., through eddy motion. Generally the motion of the atmospheric eddies, which are composed of a range of sizes in the atmospheric surface layer, are produced by various mechanisms which may be classified conveniently as follows\*:

- 1) eddy motion of a large scale. . . , which has mainly a scale associated with perturbations related to such motions as a cyclone, an anticyclone, and front;
- 2) eddy motion of a meso-scale. . . , which has a scale created by disturbances such as a tornado and thunderstorm cells;
- 3) eddy motion of a local scale. . . , which is produced by obstructions such as local hills or mountains;
- 4) eddy motion of a micro-scale. . . , which is created by roughness (which is a smaller scale than a local scale, for example) including woodland, canopies of vegetation and small protuberances of the surface, etc., of the earth's surface.

---

\* they are mixed with each other and there is no distinct identification

The above-mentioned eddies are maintained through the supply of energy from wind shear and buoyancy. All eddies contribute to the dispersion of matter or heat injected in the atmospheric flow. Thus, the scale of eddies for a wide range in atmospheric diffusion needs to be taken into consideration. It may be said, however, that much attention is directed to the scale smaller than the local scale for the study in a wind tunnel, at least quantitatively up to the present. This means that there is no variation of mean wind direction. Usually the variation of mean wind direction may often be created by the meso or large scale eddy motion.

Behavior of a smoke plume under the variation of the mean wind direction is sometimes called a meandering phenomena, which makes a complex problem for study. As of this time, there is not enough information on it. Therefore, the discussion of similarity criteria for turbulent diffusion, which follows, excludes the meandering phenomena.

So far many studies of turbulent diffusion have been confined to flows having neutral stratification. However, ordinarily neutral stratification occurs but twice daily in the lowest 100 m during transition between prevailing day-time regimes of negative and night-time regimes of positive stability. It is, therefore, of considerable practical interest to assess the influence exerted upon the turbulent diffusion process by conditions of fluid stability other than those of neutral stratification.

### 7.1. Small-Scale Diffusion

For non-neutral stratification it may be shown (Batchelor 1953)<sup>34</sup> that dynamical similarity of flows, with geometrically similar boundary conditions, is defined quantitatively by the three scale  $V$ ,  $L$ ,  $\theta$  referring to velocity variation, length, and potential temperature--  
 $V, L / \nu$  (Reynolds number),  $g\theta, L / (T V^2)$  (Richardson number), and  $\frac{k}{C_p \mu}$  (Prandtl number). For flows of essentially the same gas (for instance the air in the present case) the Prandtl number does not vary and experience for shear flows of high Reynolds number shows that viscosity has no effect on the scale components of the motion which contains nearly all the energy that might contribute effectively to turbulent diffusion. Thus, it follows that similarity depends only on the scale Richardson number. Thus, it is required that a length scale be sought which is related to the Richardson number for similarity of turbulent diffusion. Current practice utilizes a length scale incorporating a stability length  $L$  which is a unique function of  $Ri$  by means of  $z/L$ , here  $z$  is the height above the surface and/or denotes the characteristic height of the phenomena.

Thus, similarity criteria of turbulent diffusion requires the following conditions:

- 1) for geometrical similarity of boundaries, where  $M$  and  $P$  denote, respectively, the model and the prototype

$$(z_o/L)_M = (z_o/L)_P \quad (7-1)$$

where  $z_o$  is the roughness height.

- 2) for similarity of flow, profiles of mean wind speed and of mean temperature, respectively

$$f(z/L)_M = f(z/L)_P, \text{ and } \theta(z/L)_M = \theta(z/L)_P \quad (7-2)$$

in which  $f$  and  $\phi$  denote universal functions.

- 3) for characteristic height of the diffusion phenomena, for example, the boundaries of the smoke plume

$$(z/L)_M = (z/L)_P \quad (7-3)$$

- 4) for similarity at downwind locations

$$(Cx/L)_M = (Cx/L)_P \quad (7-4)$$

where  $C$  is a constant and  $x$  is the distance downwind from a source.

Besides the requirement of similarity between the vertical profiles of mean velocity for the model and prototype various investigators have determined additional requirements which are necessary for diffusion similarity. Inoue<sup>16</sup> was able to show that when diffusion occurs within a velocity profile which is logarithmic, the parameters  $h/z_o$  and  $h/L$  must both be equal for the model and prototype

for similarity of the diffusion field. The parameters  $h/z_o$  represents the ratio of source height to the roughness length  $z_o$  which in turn is a measure of the scale of turbulence at ground level. Cermak (1963)<sup>35</sup> using the concept of Lagrangian similarity was able to relate certain statistical characteristics of the steady-state diffusion process by functional relationships to the similarity parameters  $h/z_o$ ,  $z_o/L$  and  $Cx/L$  for flow over plane surfaces. The mean velocity profiles were taken to be the logarithmic form for neutral flow and an experimental function as proposed by Swinbank for the non-neutral flows. Characteristic of the diffusion process thus related to flow characteristic were the exponents of the downwind distance  $x$  giving the downwind variation of the maximum mean ground-level concentrations  $C(x, o, o)$ , plume width  $b(x, -, o)$  and plume height  $h_p(x, o, -)$ .

Thus, one has functional forms for

$$\begin{aligned}
 C(x, o, o) &= f_1 \left( \frac{h}{z_o}, \frac{z_o}{L}, \frac{Cx}{z_o} \right) \\
 b(x, -, o) &= f_2 \left( \frac{h}{z_o}, \frac{z_o}{L}, \frac{Cx}{z_o} \right) \\
 h_p(x, o, -) &= f_3 \left( \frac{h}{z_o}, \frac{z_o}{L}, \frac{Cx}{z_o} \right)
 \end{aligned} \tag{7-5}$$

For the forms given by Cermak to be valid the range of  $\frac{Cx}{z_o}$ , as well as  $h/z_o$ , must be restricted to the lower level of the boundary layer where the velocity profiles are of the form selected for analysis.

This usually restricts consideration to diffusion fields in the region  $0 \leq z / \delta < 0.4$  where  $S$  is the momentum-boundary-layer thickness. Immediately, this restriction shows the importance of creating thick turbulent boundary layers for laboratory simulation of atmospheric diffusion. Cermak (1963)<sup>12</sup> compared laboratory data and atmospheric data on diffusion which met the height limitations and formed good agreement. These comparisons are exemplified by Fig. 25 which is essentially confined to neutral thermal stratification.

Thus, the basic length scale ratio occurring in turbulent diffusion similarity considerations is that of

$$\frac{(z_0)_{\text{model}}}{(z_0)_{\text{prototype}}}$$

Unfortunately, the values of  $z_0$  are difficult to determine accurately in both the atmospheric and the laboratory. Hence, another form of reference length is desirable. Recalling that  $z_0$  represents a typical scale of turbulence, a length scale could also be determined by using a ratio of an integral scale of turbulence for the two flows. More laboratory and field data on turbulence are needed to study this concept.

To illustrate application of the foregoing concepts, consider the possibilities of simulating turbulent diffusion over a flat region of terrain where vegetation produces a roughness length of 10 cm.

A surface of roughness length 0.1 mm is placed upon the meteorological wind-tunnel floor. If a wind-speed of 3 m/sec is chosen for the wind tunnel, the boundary layer will be turbulent and, from the data in Chapter 3, the boundary-layer thickness should be about 2/3 m over the last 6 m of the test-section floor. Accordingly, for a point or line source placed at ground level in the wind tunnel about 6 m from the downstream end of the test section, simulation of the atmospheric diffusion field will be possible within the 6 m distance. The plume dimensions measured in the wind tunnel could be scaled up to prototype values by multiplying model values by

$$\frac{(z_o)_{\text{prototype}}}{(z_o)_{\text{model}}} = \frac{10}{0.01} = 1000$$

the downwind distance of 6 m in the wind tunnel would correspond to 6000 m in the field. If thermal stratification effects were to be studied, model values of the stability length  $L_{(\text{model})}$  must be related to the prototype stability length by

$$\begin{aligned} L_{(\text{model})} &= L_{(\text{prototype})} \frac{(z_o)_{\text{model}}}{(z_o)_{\text{prototype}}} \\ &= \frac{L_{(\text{prototype})}}{1000} \end{aligned}$$

Remembering the definition of  $L$ , such a relatively small value of  $L$  for the model implies that the heat transfer rate between the air and

ground surface (aluminum plate in wind tunnel) must be about 1000 times larger for the model than for the prototype. Such a difference in heat transfer rates is possible with the existing facility.

## 7.2. Meso-Scale Diffusion

Simulation of meso-scale diffusion using existing sizes of wind tunnels requires greater approximation and a different point of view than that for the small-scale simulation. Working at scales from 1:5000 to 1:50,000 implies that the Reynolds numbers, in the usual sense, will have the same ratios. However, mean-flow similarity can be closely achieved, as discussed earlier in Chapter 5, if a laminar flow model is compared with turbulent flow in the prototype.

The question which now remains is how to interpret diffusion characteristics in the laminar-flow model in terms of the turbulent-flow prototype. In cases where the surface over which the flow occurs is irregular, composed of hills and valleys, dispersion of a passive additive to the atmosphere may be controlled primarily by strong spatial variation in convective transport by the mean motion. Especially in flows with strong stable thermal stratification is this mode of dispersion expected to be dominant. The significance of this possibility may be recognized most readily by examining the turbulent diffusion equation

$$\frac{\partial \bar{C}}{\partial t} + \bar{U}_i \frac{\partial \bar{C}}{\partial x_i} = \frac{\partial}{\partial x_i} \left( \eta \frac{\partial \bar{C}}{\partial x_i} - \overline{u_i c} \right) \quad (7-6)$$

When the mean flow is steady, a convective dominated transport system would then be described by

$$\bar{U}_i \frac{\partial \bar{C}}{\partial x_i} = 0 \quad (7-7)$$

Accordingly, the non-dimensional form for this conservation of mass statement is merely

$$\bar{U}'_i \frac{\partial \bar{C}'}{\partial x'_i} = 0$$

This implies, since no coefficients of scale factors enter the equation, the only conditions necessary for similarity of the concentration field is that of geometrical similarity and mean velocity similarity which must be attained by meeting the conditions for dynamic similarity. Much work remains to establish the extent to which the foregoing arguments can be exploited for practical applications. The only known study of this nature is the exploratory work on simulation of mean winds and diffusion for strong inversions over Point Arguello, California, in which a 1:12,000 scale model was employed (Ref. 22). In this work a stably stratified laminar flow over the laboratory model yielded, as stated in Chapter 5, mean wind patterns which simulated actual wind patterns in their general character. Therefore, if convective spreading controls the dispersion of contaminants, reasonable agreement between diffusion in the Point Arguello model and prototype should be found.

An attempt to check the diffusion characteristic in the laboratory and field was made for the Point Arguello study. Helium was released as a laboratory tracer in Hondo Canyon at the location where fluorescent particles were released in the field. Figure 15 shows a comparison of the trajectory for the tracer in the laboratory and field. Excellent agreement exists for this particular characteristic. In Fig. 26, a comparison is made of the way in which concentration levels decrease with distance from the source. Unfortunately, the field data show considerable scatter which does not permit drawing a strong conclusion on similarity of the two diffusion fields. However, a significant feature associated with the data is that the decrease in concentration with distance downwind from the source is nearly the same in both cases. The distances associated with the model were scaled up by a factor of 12,000 to yield a comparison with the prototype.

Although the type of similarity considered in this section appears to be based on radical simplifications, the results obtained to date are sufficiently satisfactory to warrant further research on this modeling concept. Satisfactory modeling techniques of this nature have great potential for the study of practical dispersion problems.

## REFERENCES

1. Abe, M., Mountain clouds, their forms and connected air currents, Part II, Bull. Centr. Met. Obs., Japan 7(3), 1941.
2. Chopra, K. P., and L. F. Hubert, Kármán vortex sheets in wake of islands. Paper No. 65-16, AIAA 2nd Aerospace Sciences Meeting, New York, January 1965.
3. Field, J. H. and R. Warden, A survey of air currents in the Bay of Gibraltar, 1929-1930. Geophysical Memoirs, No. 59 (R and M 1563) Published by Her Majesty's Stationery Office.
4. Cermak, J. E., R. C. Maholtra, and E. J. Plate, Investigations of the Candlestick Park wind problem, Vol. II: Wind-tunnel model study, Fluid Dynamics and Diffusion Laboratory, Report No. 63 JEC-RCM-EJP27, Colorado State University, July 1963.
5. Lumley, J. L. and H. A. Panofsky, The structure of atmospheric turbulence. Interscience, 1964.
6. Townsend, A. A., The structure of turbulent shear flow. Cambridge University Press, 1956.
7. Plate, E. J. and J. E. Cermak, Micrometeorological wind-tunnel facility. Final Report, Contract No. DA-36-039-56-80371. For U.S. Army. Fluid Dynamics and Diffusion Laboratory Report No. CER63 EJP-JEC9, Colorado State University, February, 1963.
8. Plate, E. J. and J. E. Cermak, Investigations to develop wind-tunnel techniques for measuring atmospheric gaseous diffusion in model vegetative surfaces. Final Report on Contract No. 12-14-100-4546(41) U.S. Department of Agriculture. Fluid Dynamics and Diffusion Laboratory Report CER63 EJP-JEC28, Colorado State University, July 1963.
9. Schlichting, H., Boundary layer theory, McGraw-Hill Book Company, Inc., New York, 1960.

## REFERENCES - Continued

10. Plate, E. J. and A. A. Quraishi, Modeling of velocity distribution inside and above tall crops. *Journal of Applied Meteorology* Vol. 4, No. 3, pp. 400-408.
11. Plate, E. J. and C. W. Lin, The velocity field downstream from a two-dimensional model hill. Part I. Final Report on Grant No. DA-AMC-36-039-63-G7, Fluid Dynamics and Diffusion Laboratory Report No. CER63-EJP14, Colorado State University, February 1965.
12. Cermak, J. E., Lagrangian similarity hypothesis applied to diffusion in turbulent shear flow. *Journal of Fluid Mechanics*, Vol. 15, No. 1, pp. 49-64, 1963.
13. Cermak, J. E. and H. J. Koloseus, Lake Hefner model studies of wind structure and evaporation. Final Report Part I and II, Contract NObsr-57053, Bureau of Ships, U. S. Navy, Colorado State University Report No. CER54JEC20, November 1953.
14. Worthington, Skilling, Helle, and Jackson,\* World Trade Center-- wind program (Interim Reports), 1965. \*Prepared by
15. Hsi, G. and J. E. Cermak, Meteorological-tower induced wind-field perturbations. Fluid Dynamics and Diffusion Laboratory Report No. CER65GH-JEC49, Colorado State University, October 1965.
16. Inoue, E., The effects of thermal stratification on turbulent diffusion in the atmospheric surface layer. *Advanc. Geophys.*, 6, 319-330, 1959.
17. Malhotra, R. C. and J. E. Cermak, Mass diffusion in neutral and unstably stratified boundary layer flows, *Int. J. Heat and Mass Transfer*, Vol. 7, pp. 169-186, 1964.
18. Davar, K. S. and J. E. Cermak, Characteristics of diffusion plumes for a point source within a turbulent boundary layer, *Int. J. Air Water Poll*, Vol. 8, pp. 339-354, 1964.
19. Poreh, M. and J. E. Cermak, Study of diffusion from a line source in a turbulent boundary layer. *Int. J. Heat and Mass Transfer*, Vol. 7, pp. 1083-1095, 1964.

## REFERENCES - Continued

20. Yano, M., Turbulent Diffusion in a simulated vegetative cover. Ph. D. Thesis Fluid Mechanics Program, Colorado State University, 1966.
21. Plate, E. J. and C. M. Sheih, Diffusion from a continuous point source into the boundary layer downstream from a model hill. Fluid Dynamics and Diffusion Laboratory Report No. CER65EJP-CMS60, Colorado State University, December 1965.
22. Cermak, J. E. and J. A. Peterka, Simulation of wind fields over Point Arguello, California by wind tunnel flow over a topographical model. Final Report U.S. Navy Contract N126(61756)34361A (PMR). Fluid Dynamics and Diffusion Laboratory Report CER65JEC-JAP64, Colorado State University, December 1965.
23. Cermak, J. E. and R. N. Meroney, Wind tunnel modeling of flow and diffusion over San Nicolas Island. Progress Report for 4th and 5th Quarters on Contract N123(61756)-50192A(PMR), November, 1965.
24. Alaka, M. A. ed., P. Queney, et.al., The air flow over mountains. Technical Note No. 34, World Meteorological Organization, 134 p.
25. Long, R. R., A laboratory model of air flow over the Sierra Nevada Mountains. The Rossby Memorial Volume, p. 372-380.
26. Barad, M. L. ed., Project Prairie Grass, a field program in diffusion. Geophys. Res. Paper No. 59, Air Force Cambridge Research Center (1958).
27. Kolmogoroff, A., The local structure of turbulence in incompressible viscous fluids for very large Reynolds numbers. Comp. Rend. Acad. Sci. URSS, Vol. XXX, No. 4, 1941.
28. Pond, S., R. W. Stewart, and R. W. Burling, Turbulence spectra in wind over waves. Journ. of the atmospheric Sci., Vol. 20, 1963.

## REFERENCES - Continued

29. Davenport, A. G., The relationship of wind structure to wind loading, Symposium No. 16, Wind effects on buildings and structures. Vol. 1, Her Majesty's Stationery Office, London, 1965.
30. Grant, H. L., R. W. Stewart, and A. Moilliet, Turbulent spectra from a tidal channel. Journ. Fluid Mech., Vol. 12, 1962.
31. Liu, C. Y., and V. A. Sandborn, Evaluation of the turbulent energy dissipation from time derivative measurements. Research Memo, No. 5, Colorado State University, 1965.
32. Bolgiano, R., Turbulent spectra in a stably stratified atmosphere. J. Geophys. Res. 64, 2226 (1959).
33. Gurvich, A. S., Frequency spectra and distribution functions of vertical wind velocity components. Izv. Akad. Nauk. SSSR, Geophys. Ser. No. 7, p. 1042 (1960).
34. Batchelor, G. K., The conditions for dynamic similarity of motions of a frictionless perfect gas atmosphere. Q. J. R. M. S. 79, 1953.
35. Gifford, F. A., Diffusion in the diabatic surface layer. J. Geoph. Res. Paper 59, 1959.

## FIGURES

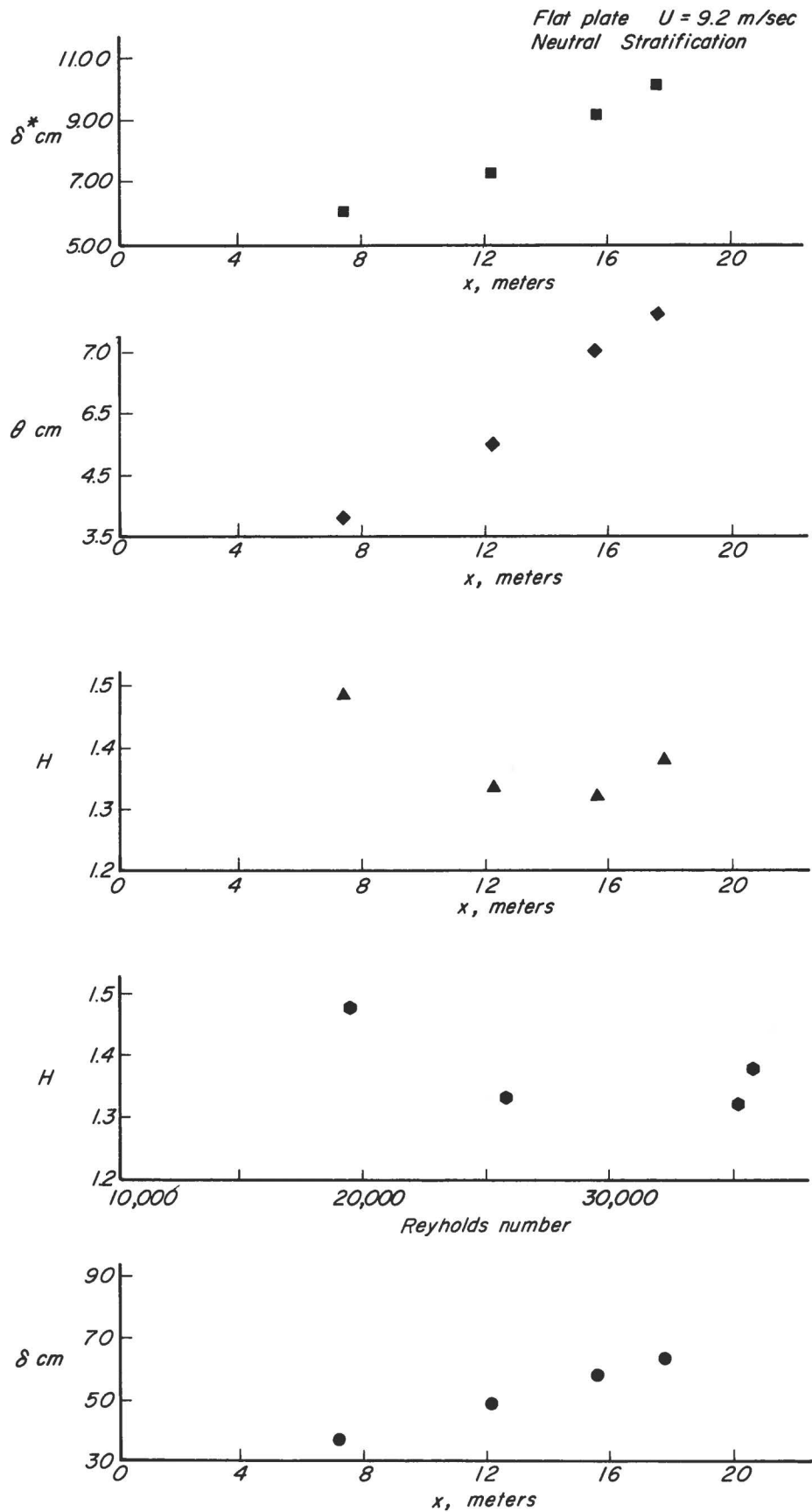


Fig. 1 Boundary characteristics for flat plate in the meteorological wind tunnel

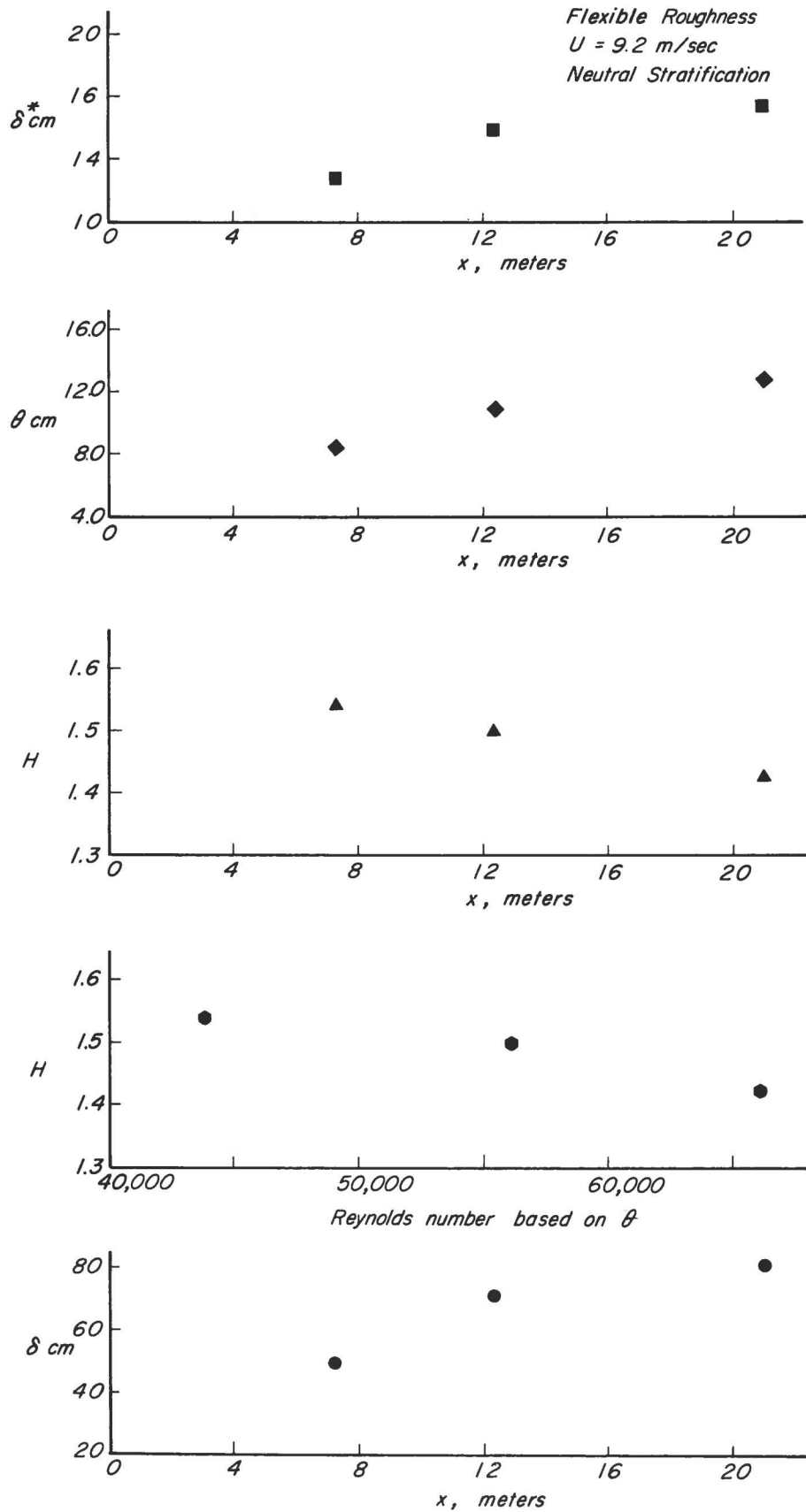


Fig. 2 Boundary characteristics for flexible roughness in the meteorological wind tunnel

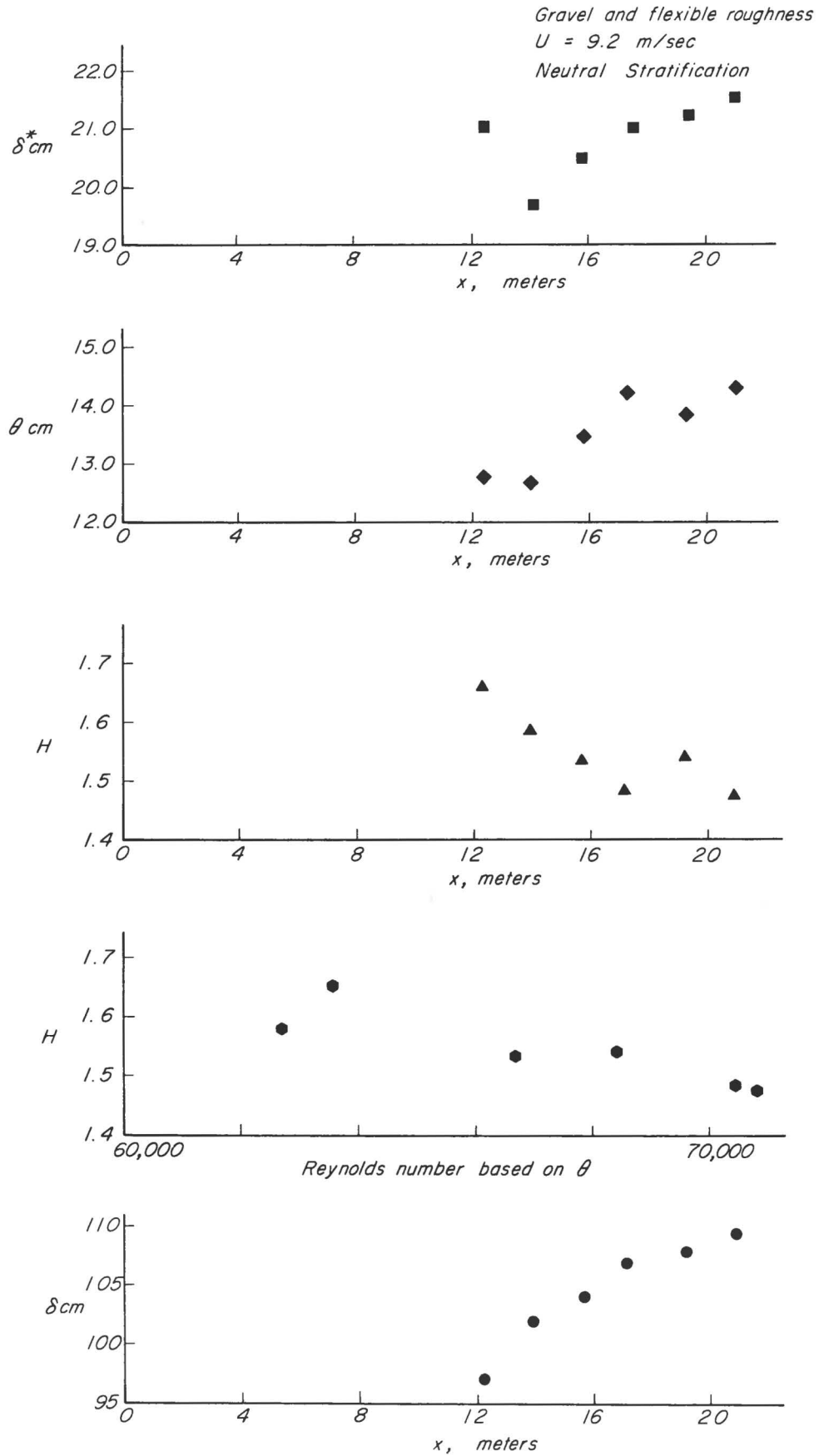


Fig. 3 Boundary characteristics for gravel and flexible roughness in the meteorological wind tunnel

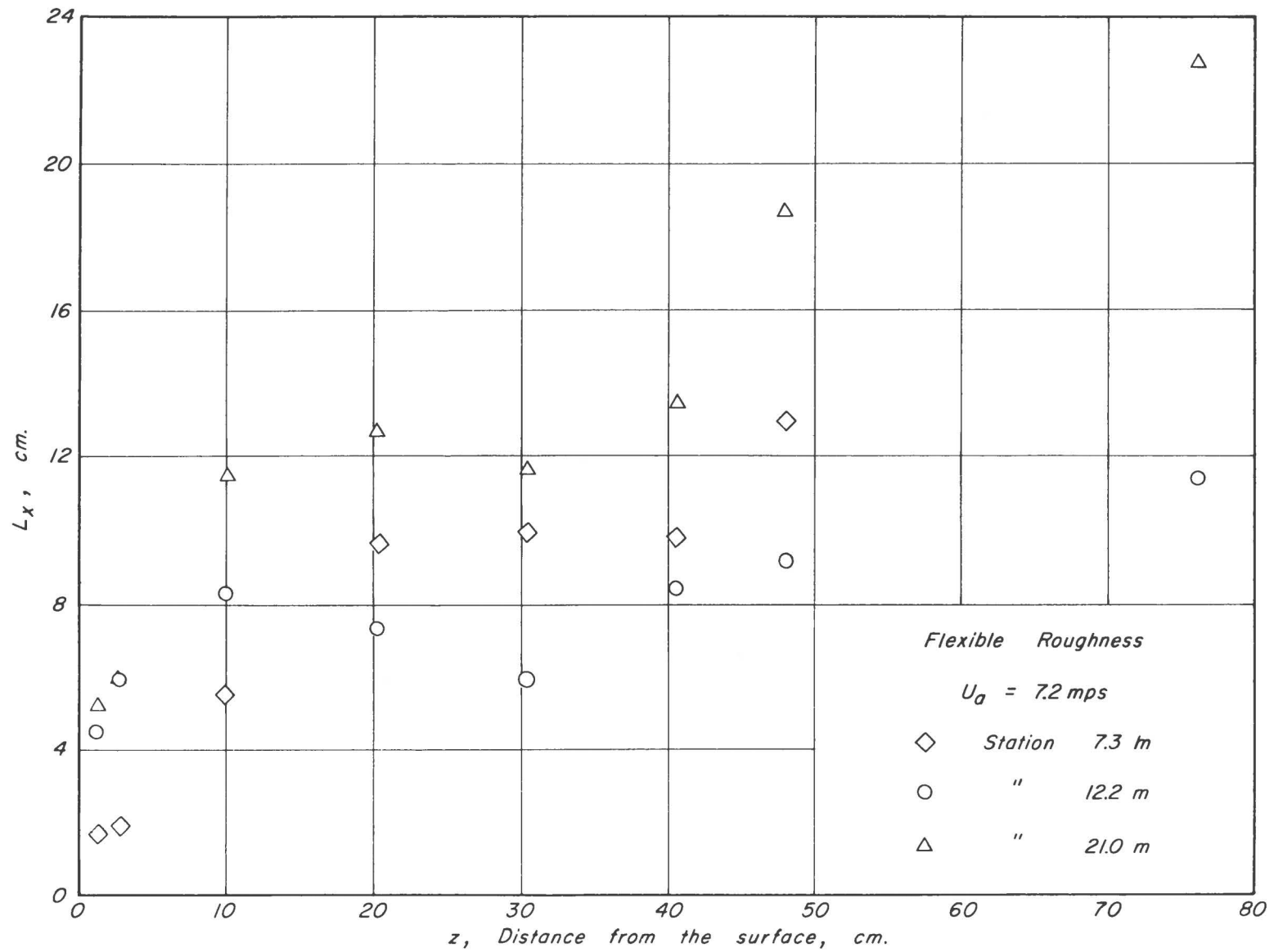


Fig. 4 Average size turbulent eddies in meteorological wind tunnel

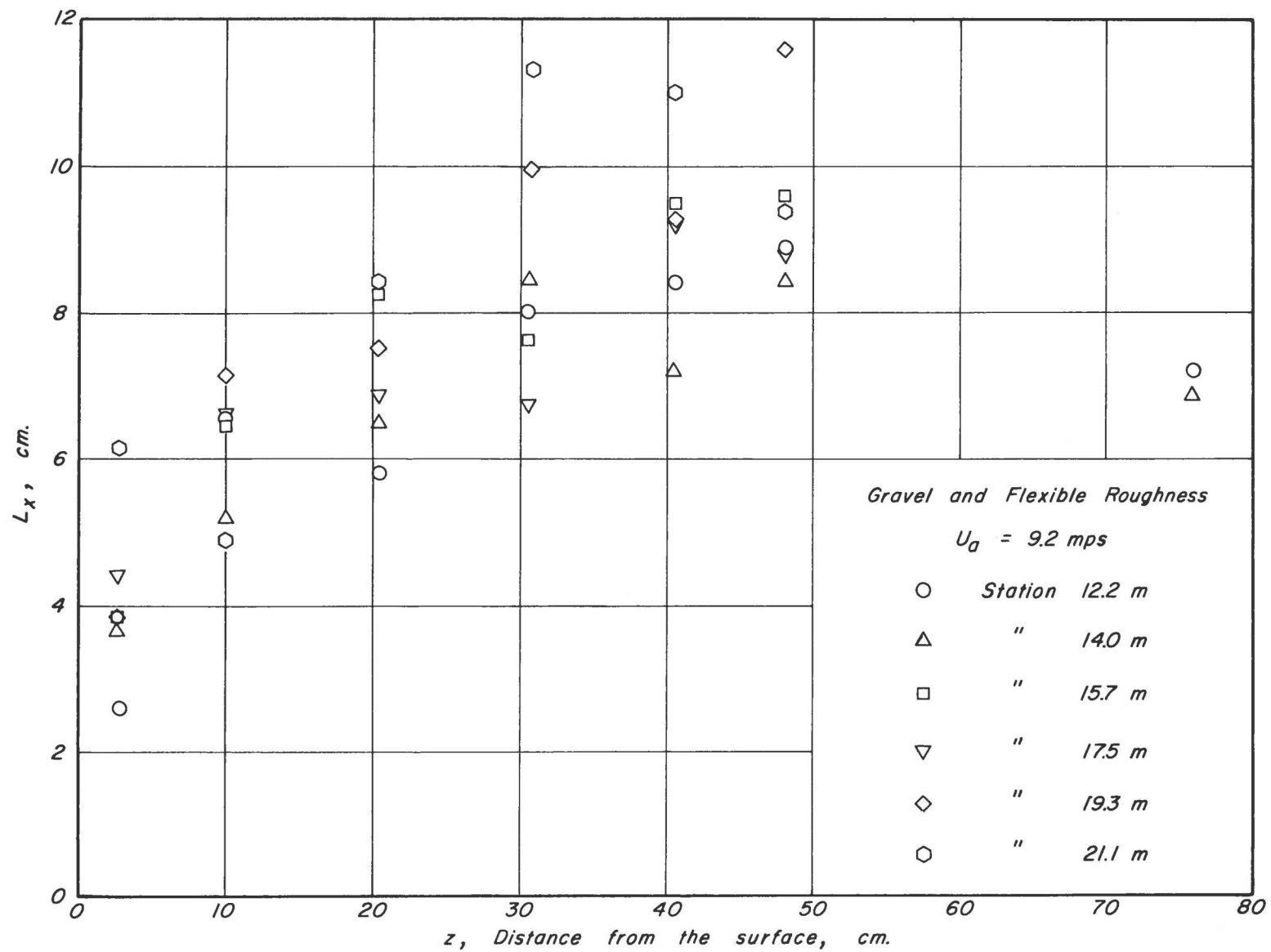


Fig. 5 Average size turbulent eddies in meteorological wind tunnel

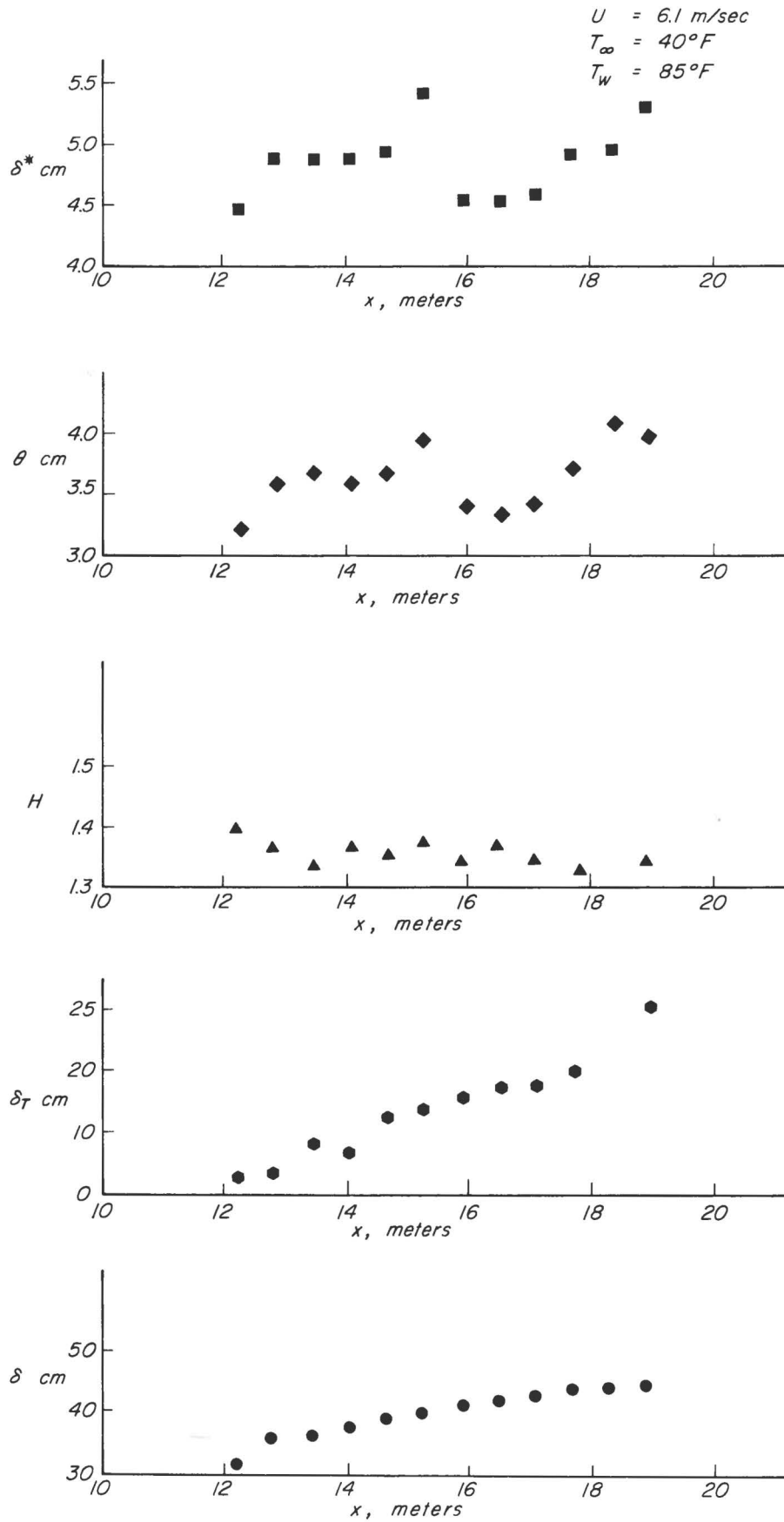


Fig. 6 Boundary characteristics for flat plate under unstable conditions in the meteorological wind tunnel

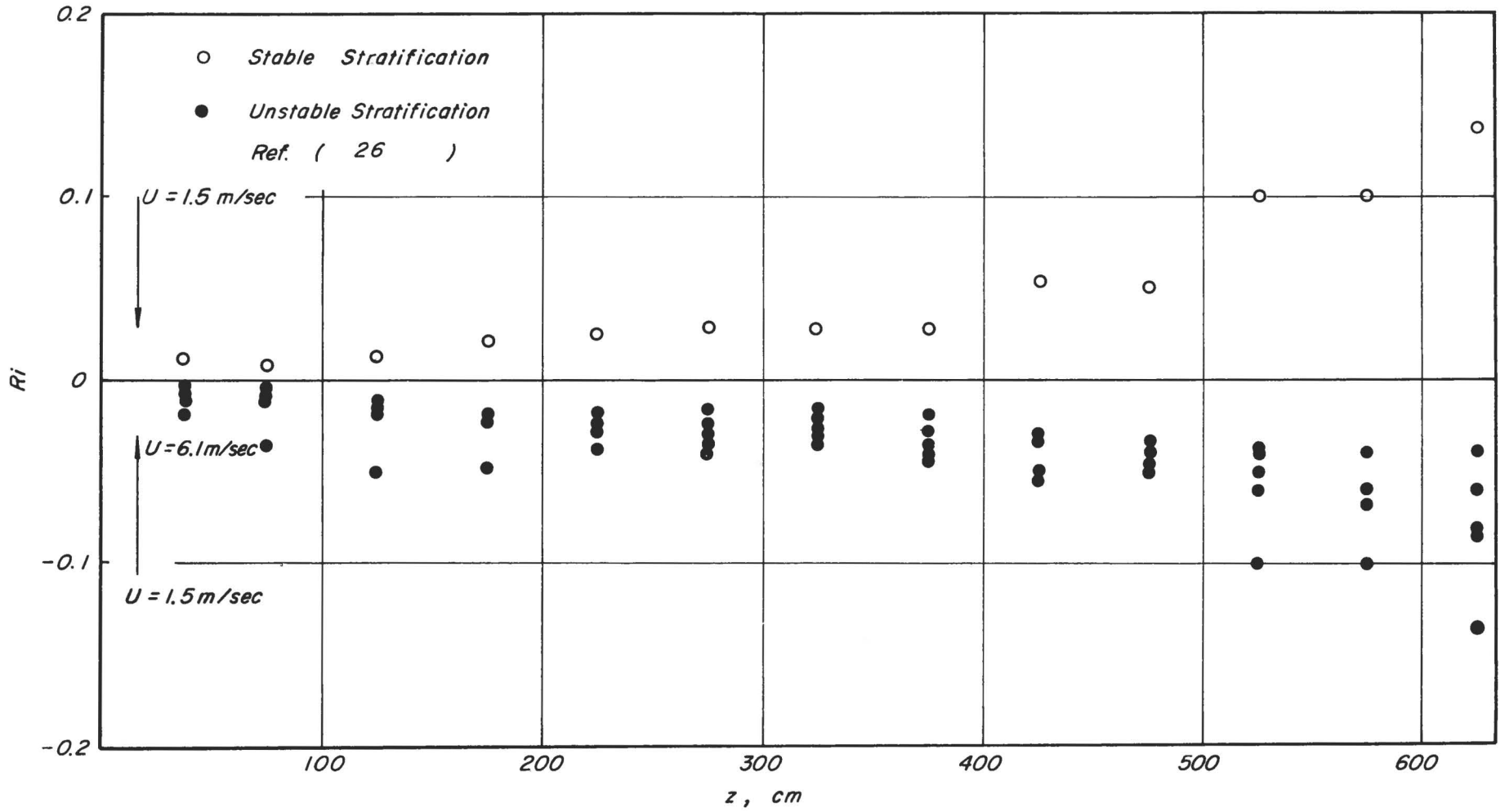


Fig. 7 Distribution of Richardson number with height in the atmosphere

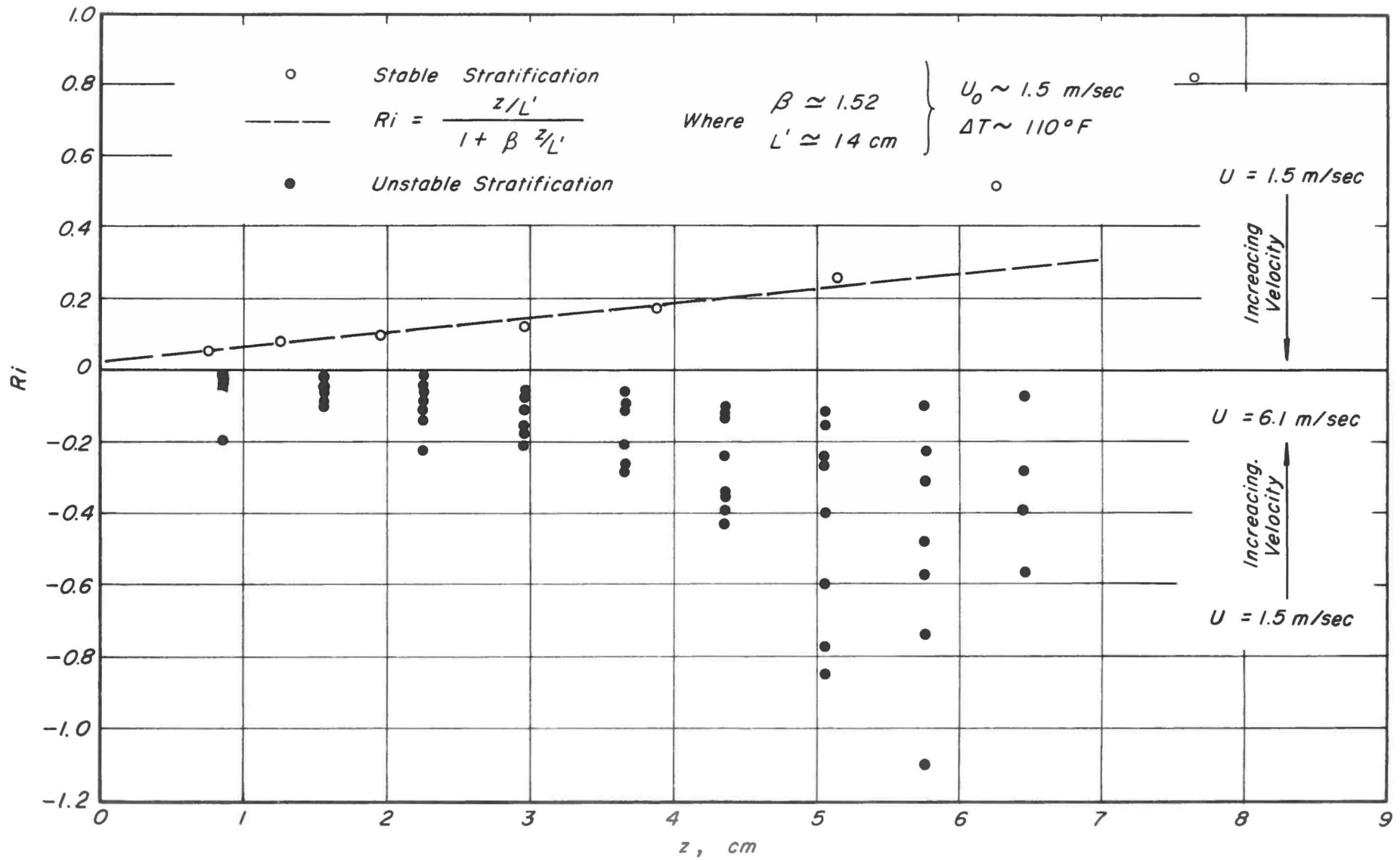


Fig. 8 Distribution of Richardson number with height in the meteorological wind tunnel

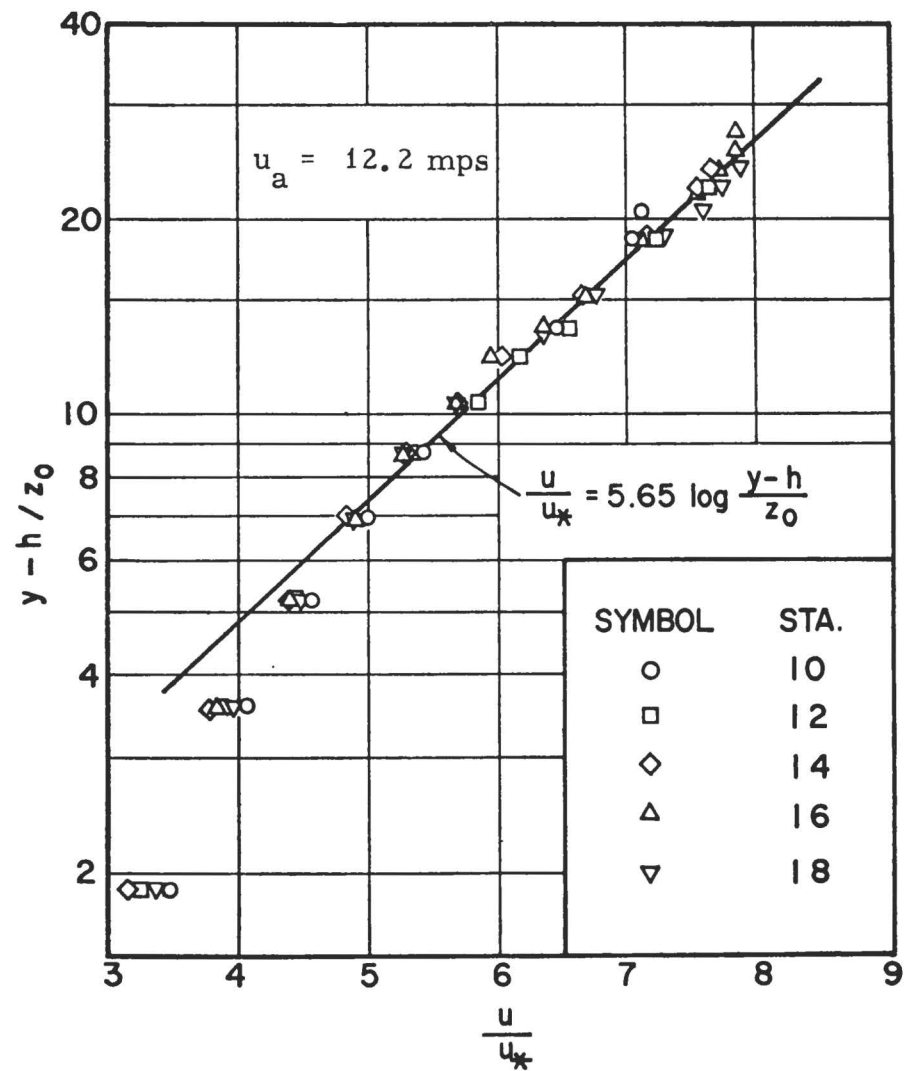
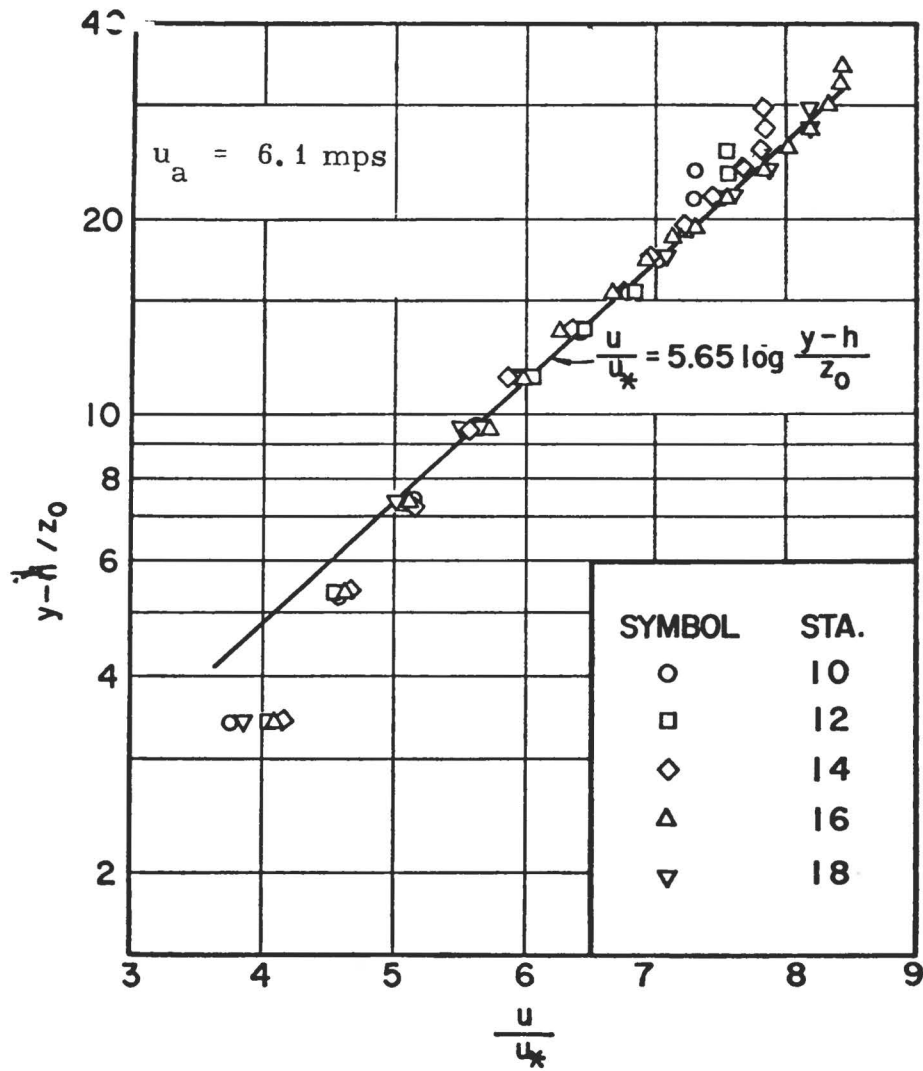


Fig. 9 Non-dimensional velocity profiles above crop: logarithmic law

STOLLER & LEMON (1963)		TAN & LING (1961)		PAESCHKE (1937)	
WHEAT		CORN		WHEAT	
Symbol	$u_h$ cm/sec	Symbol	$u_h$ cm/sec	Symbol	$u_h$ cm/sec
●	373	○	200	○	95
●	124	●	230	TAN & LING (1961)	
●	217	●	292	WHEAT	
●	287	⊕	325	Symbol	$u_h$ cm/sec
		⊗	350	△	90-300

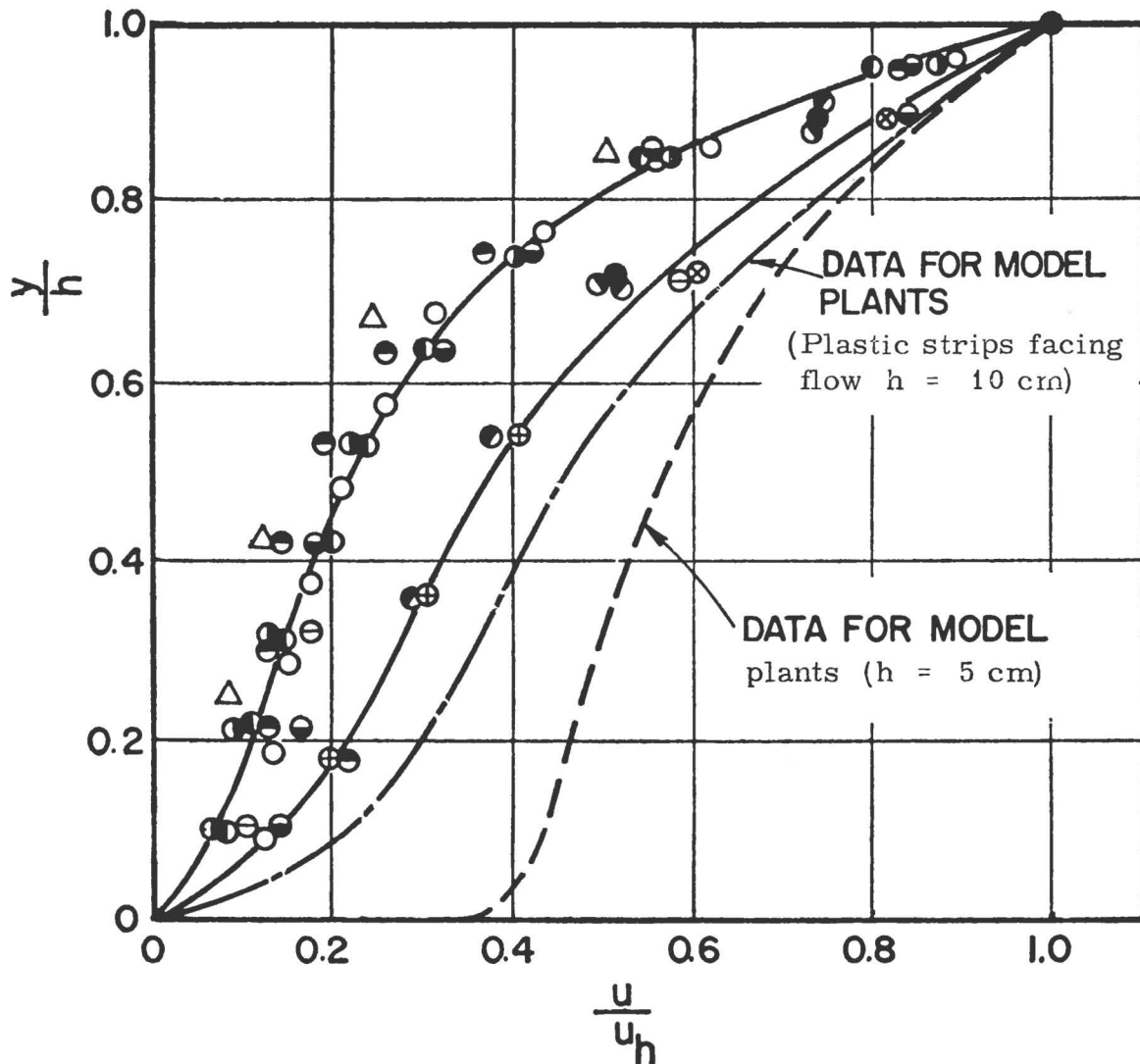


Fig. 10 Field data in canopy.

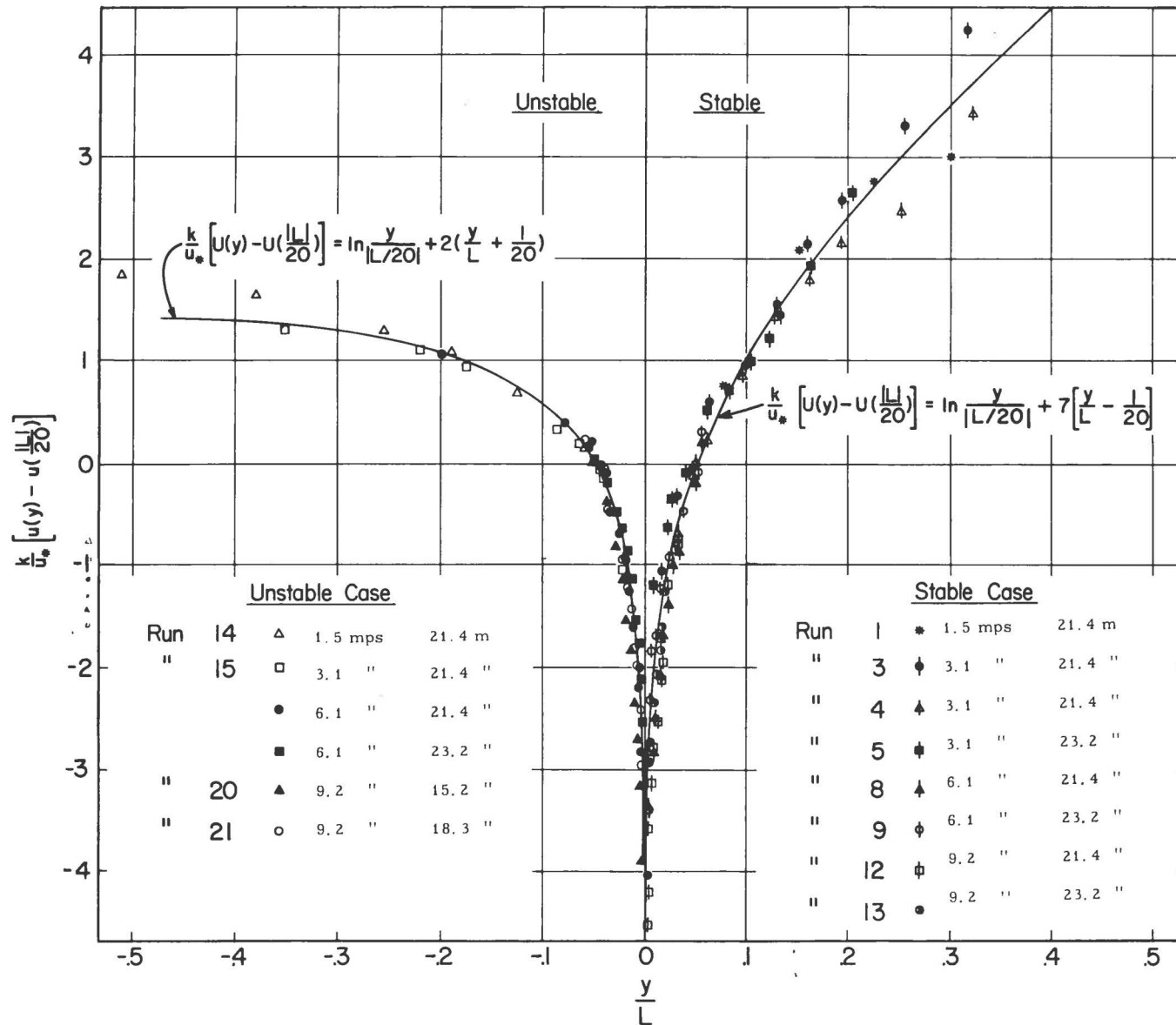


Fig. 11 Comparison of the experimental data with the universal wind profile of Monin and Obukhov

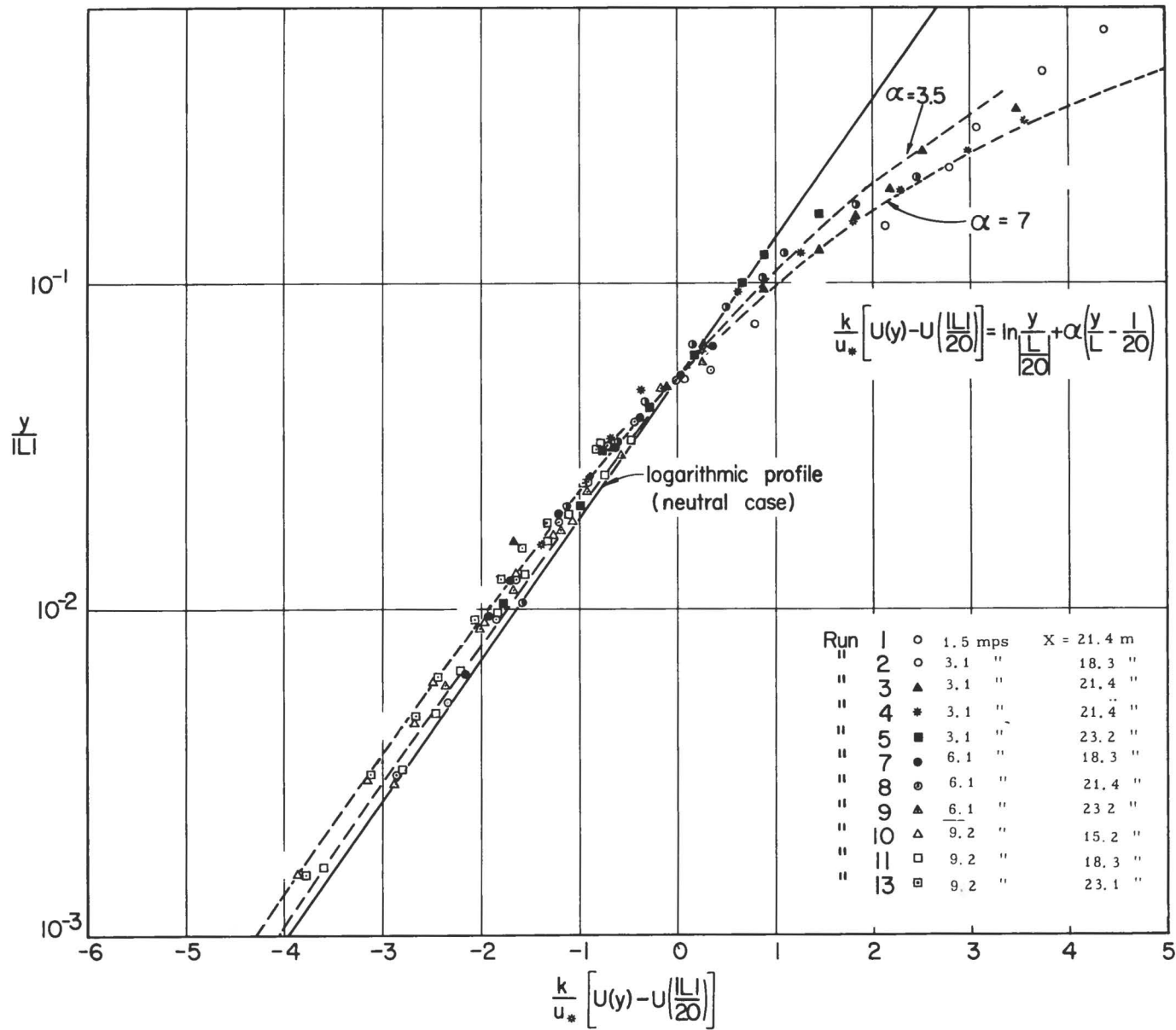


Fig. 12 Log-linear law on logarithmic scale for stable flow

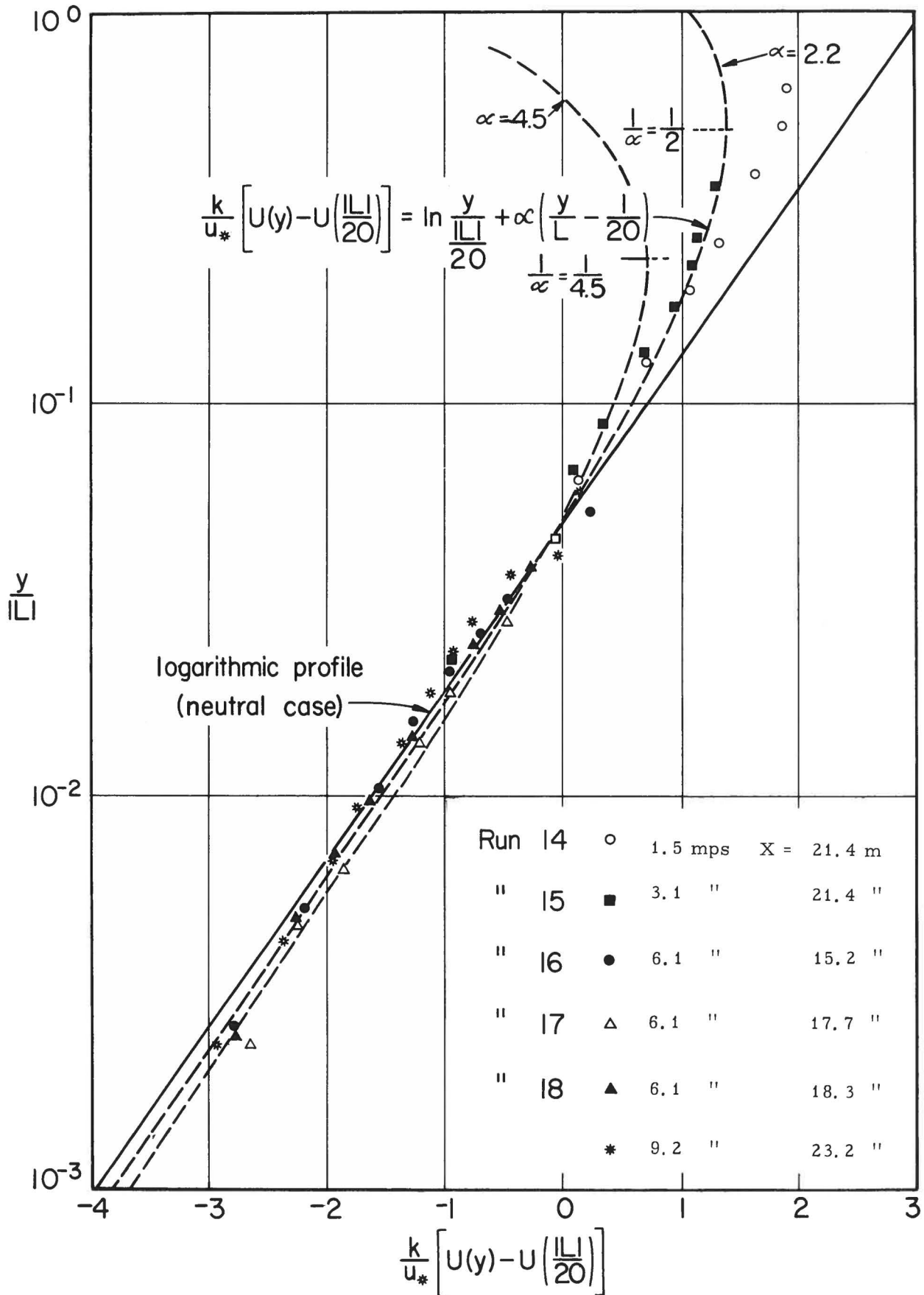


Fig. 13 Log-linear law on logarithmic scale for unstable flow

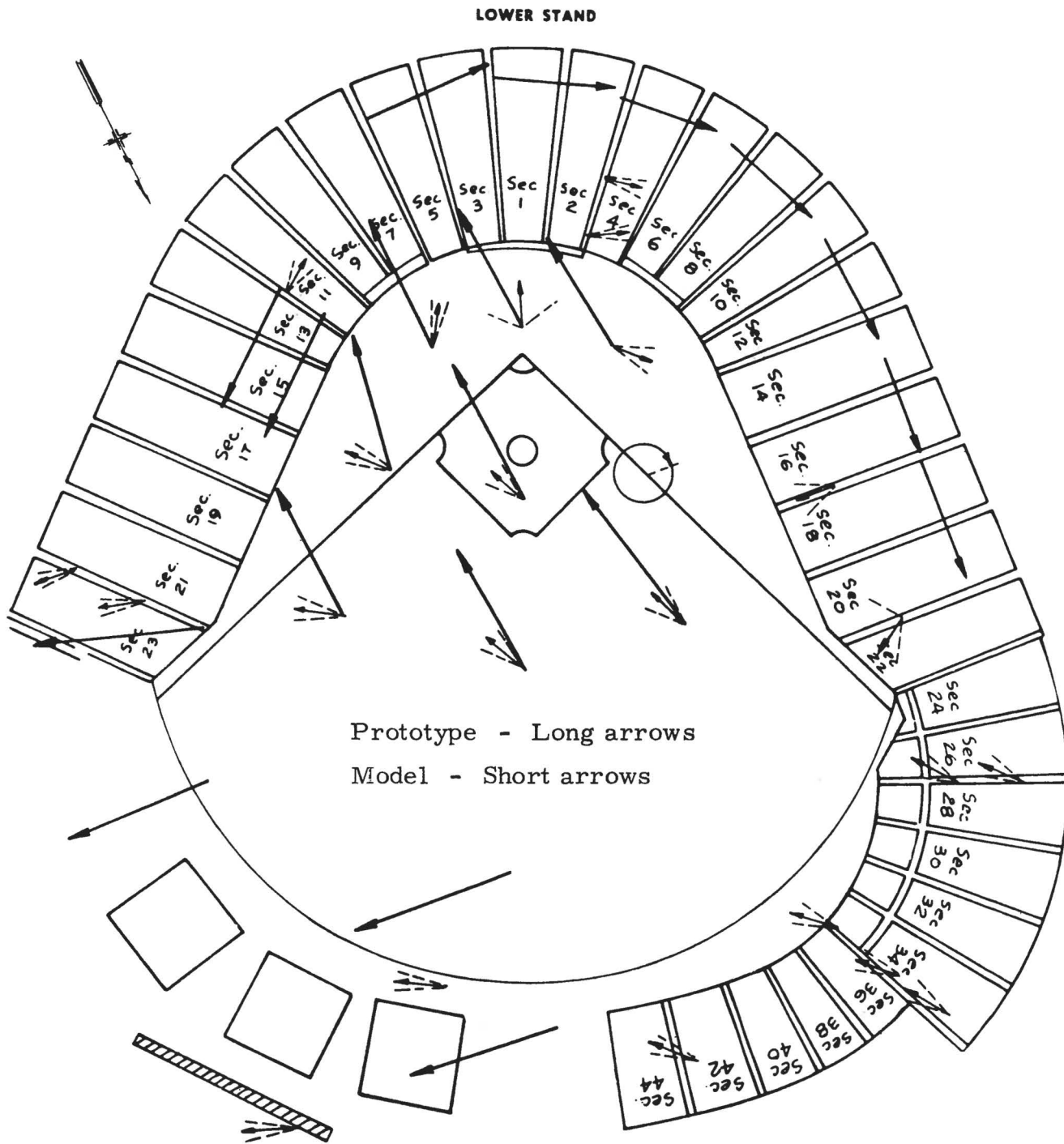


Fig. 14 Model-prototype mean flow correlation, Candlestick Ball Park (Ref. 4)

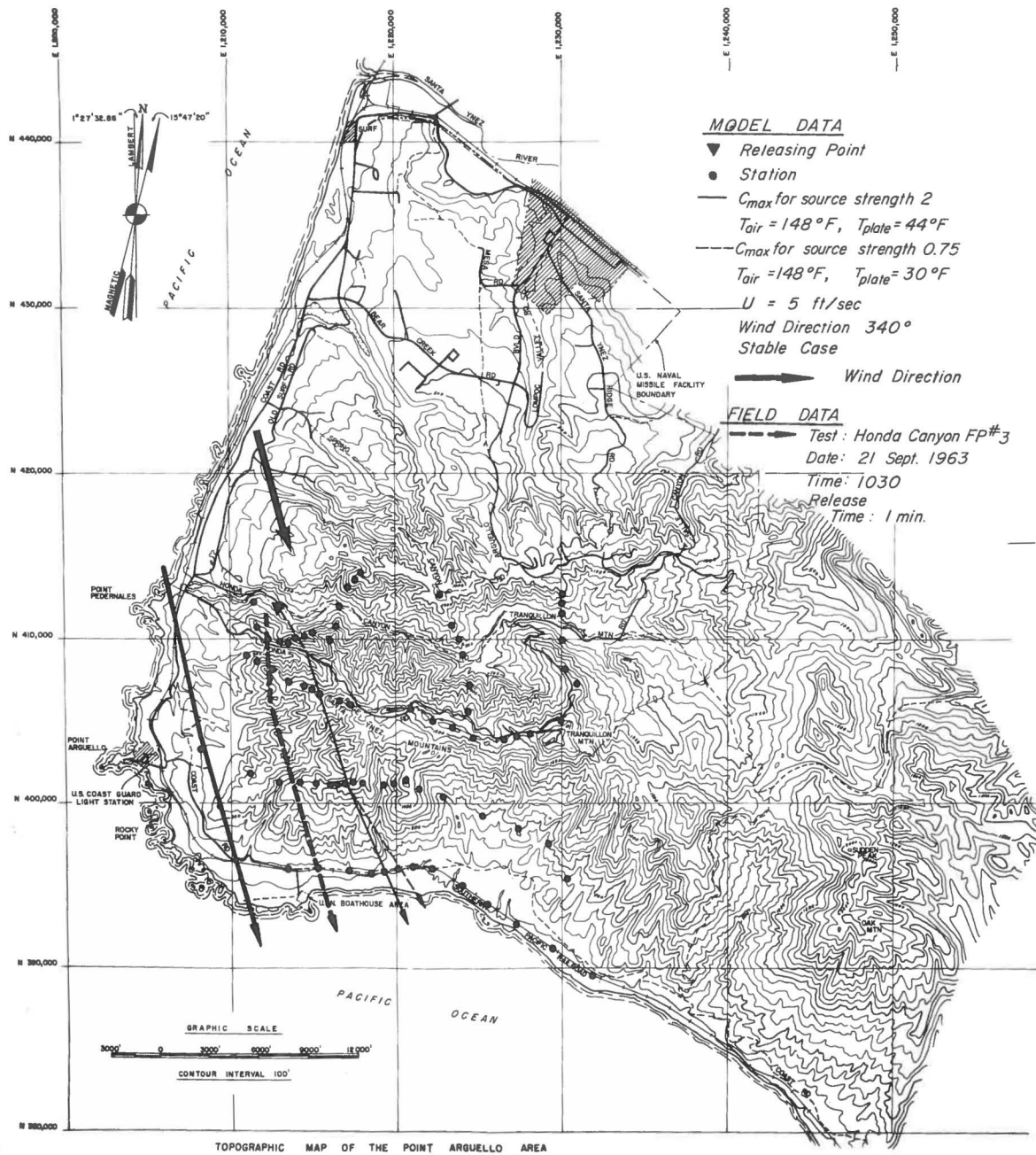


Fig. 15 Model-Prototype mean flow correlation, Point Arguello, (comparison of cloud movements from Honda Canyon for  $340^{\circ}$  winds)

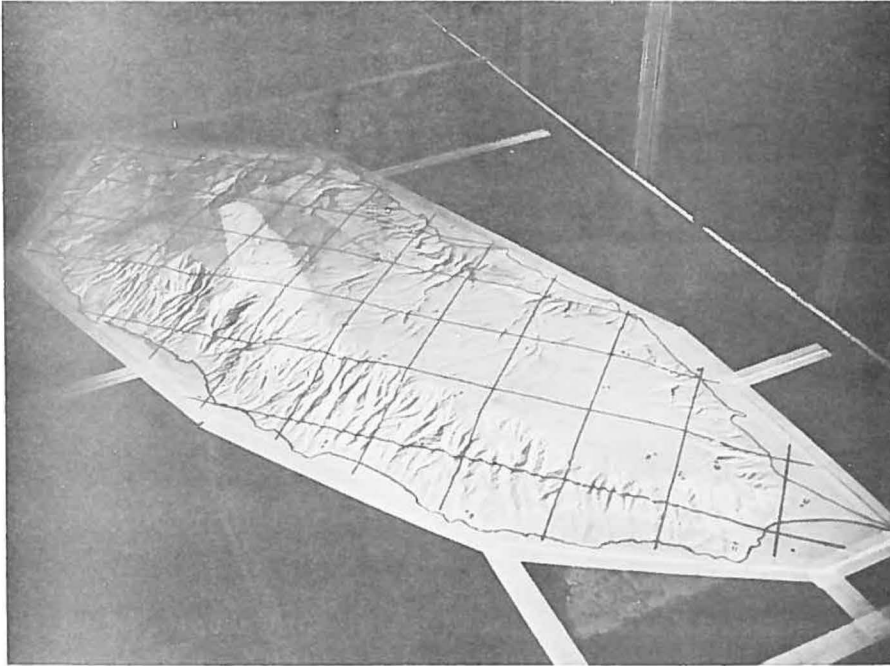


Fig. 16 Typical ammonia trace on San Nicolas Island model as mounted in meteorological wind tunnel

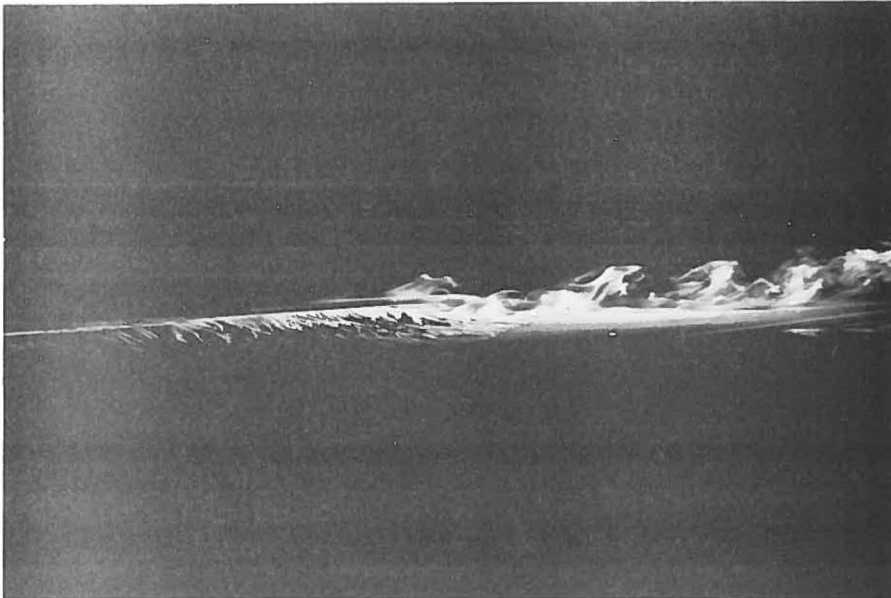


Fig. 17 Titanium - tetrachloride smoke trails in wake of San Nicolas Island model



Fig. 18 Smoke patterns over San Nicolas Island prototype

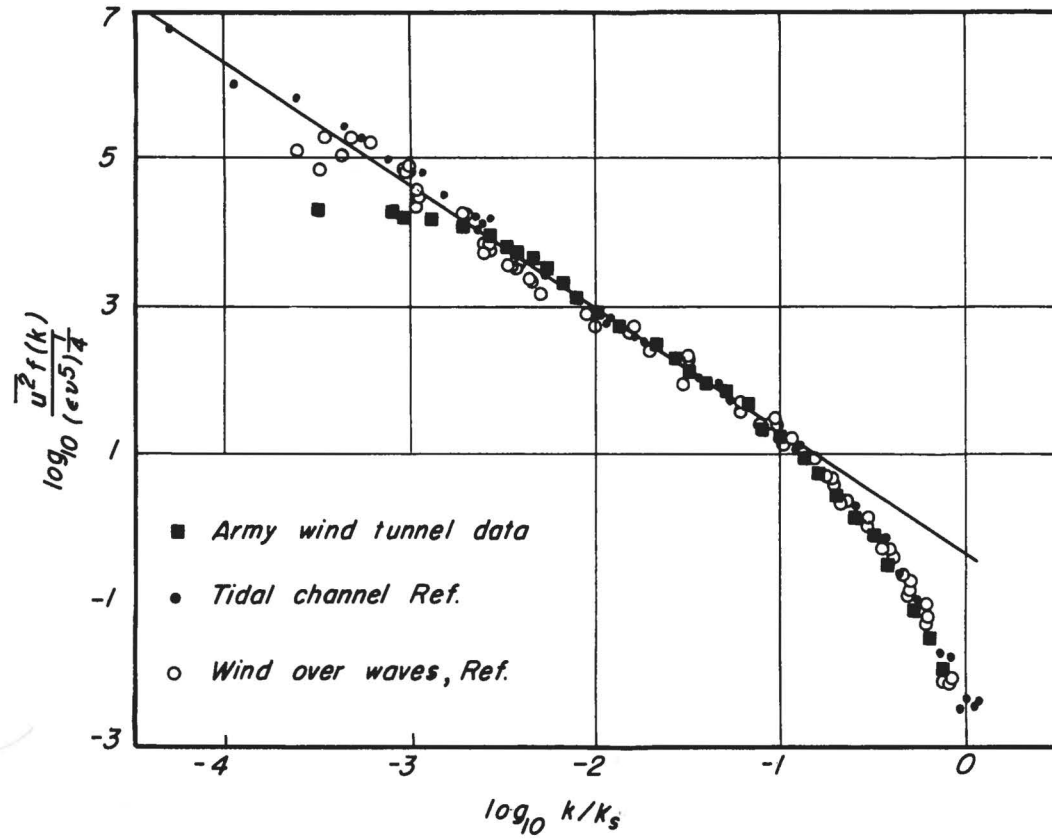


Fig. 19 Comparison of spectra measurements from the Army meteorological wind tunnel, an ocean tidal channel and air flow over the sea surface

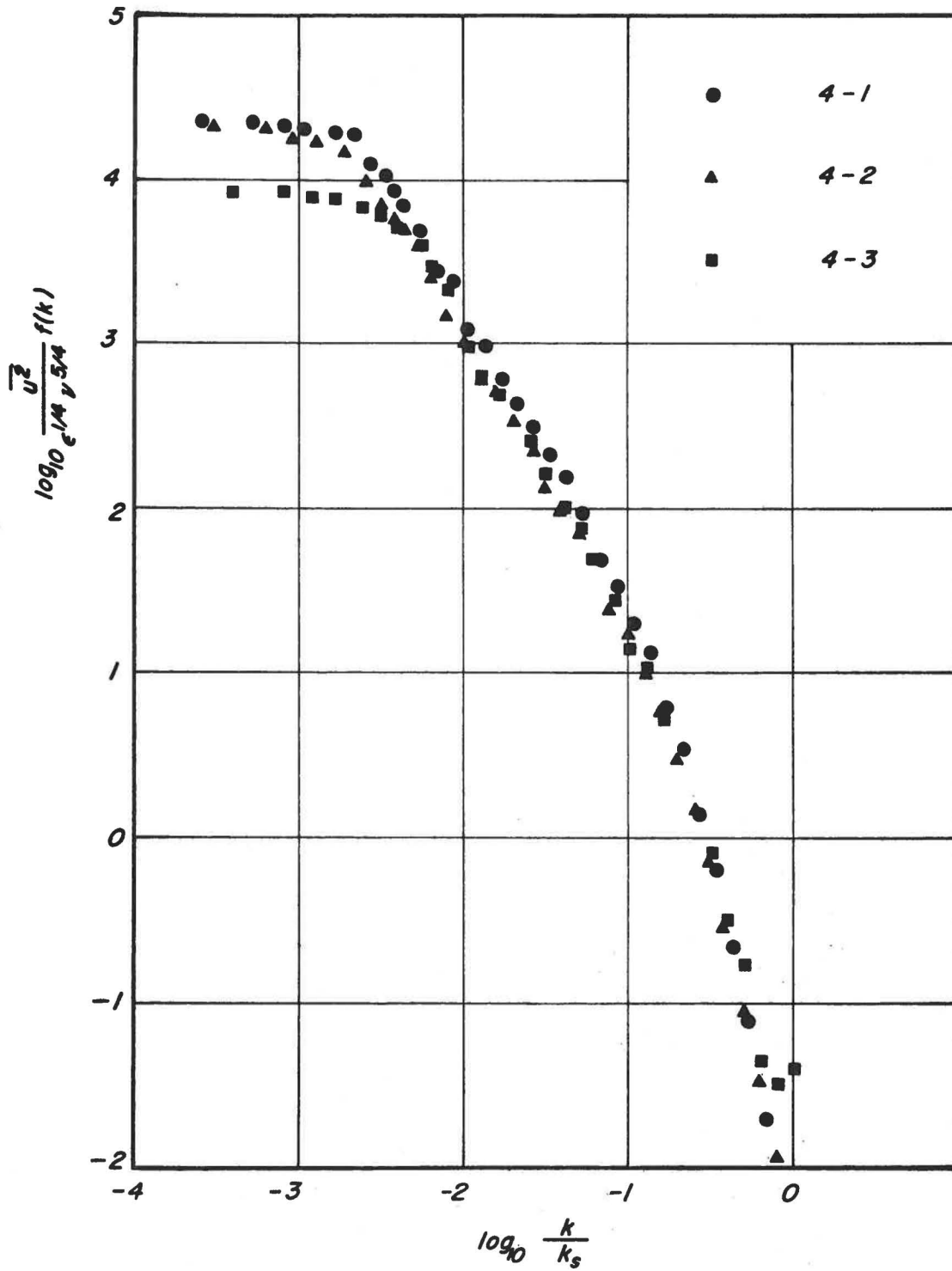


Fig. 20a Normalized energy spectra - smooth surface

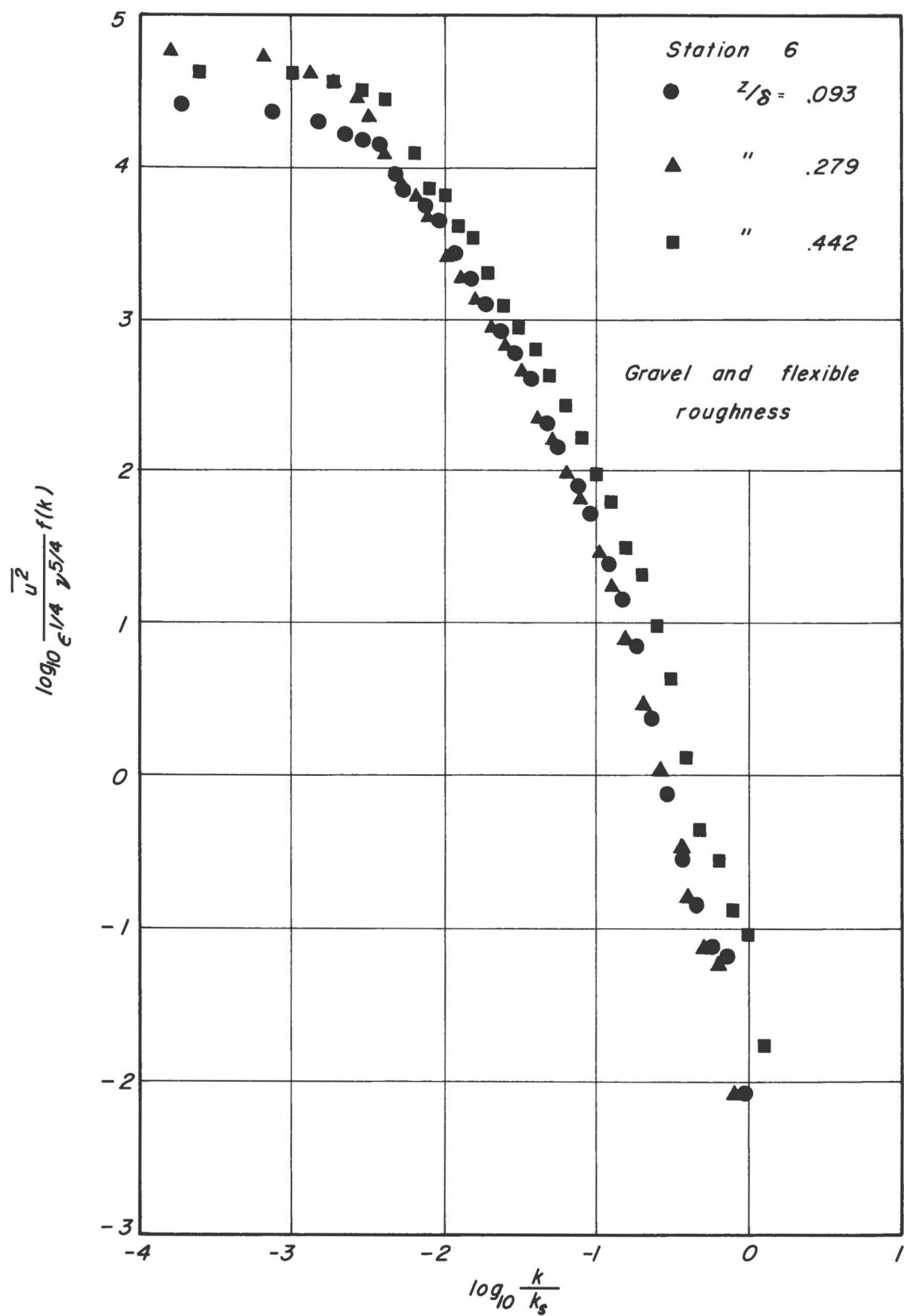


Fig. 20b Normalized energy spectra - gravel and flexible roughness

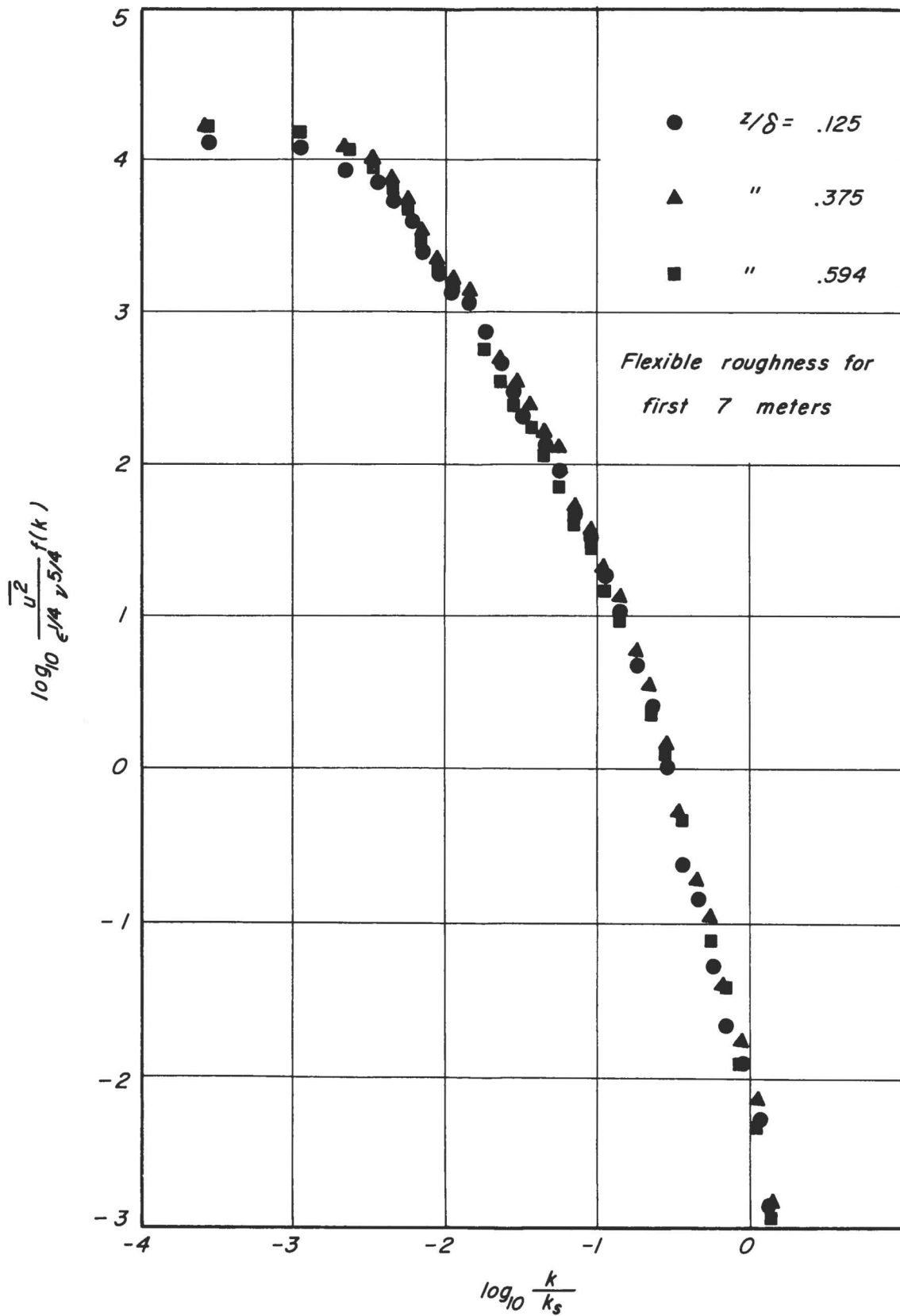


Fig. 20c Normalized energy spectra - flexible roughness

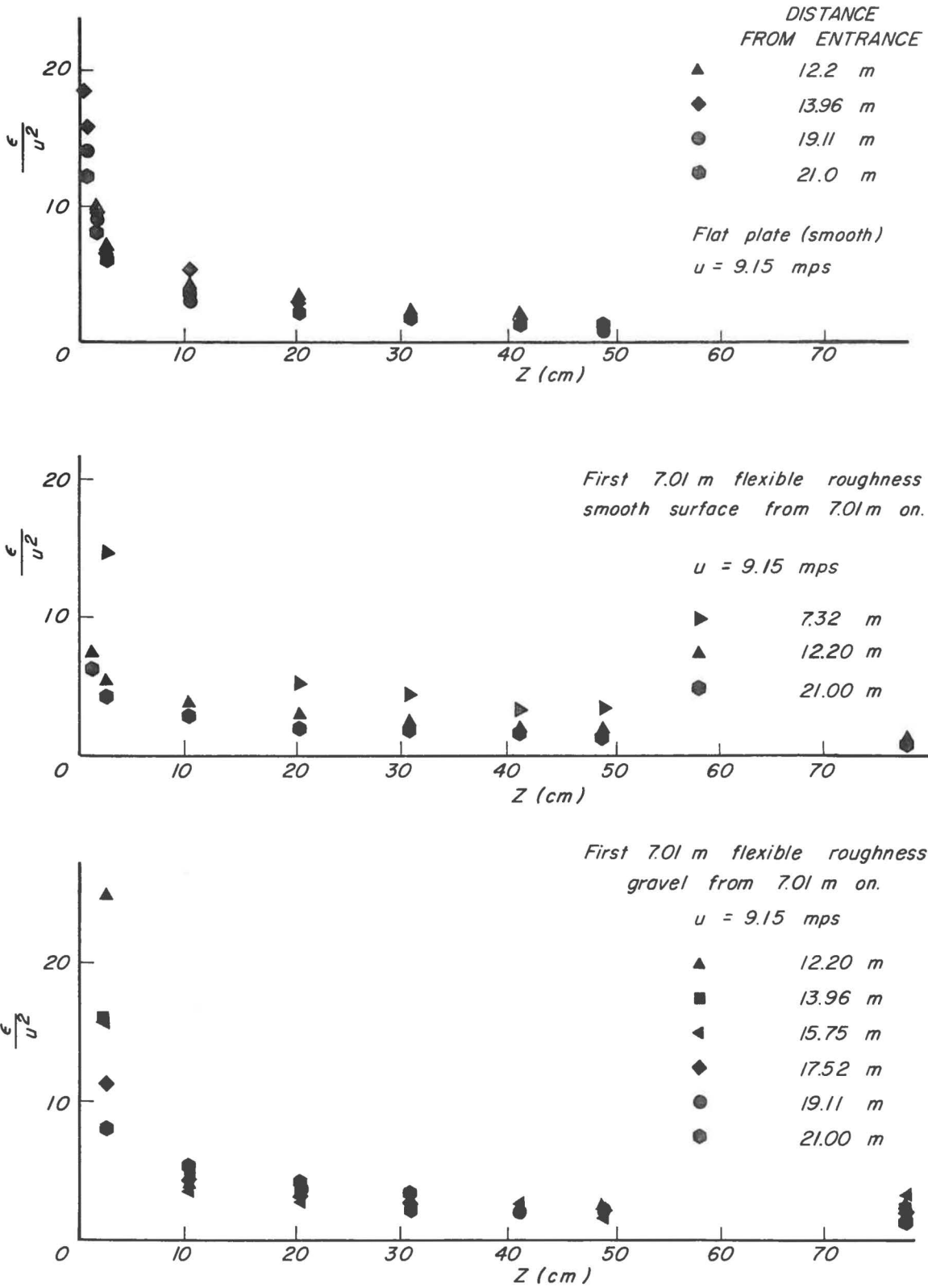


Fig. 21 Total turbulent energy dissipation in boundary layers

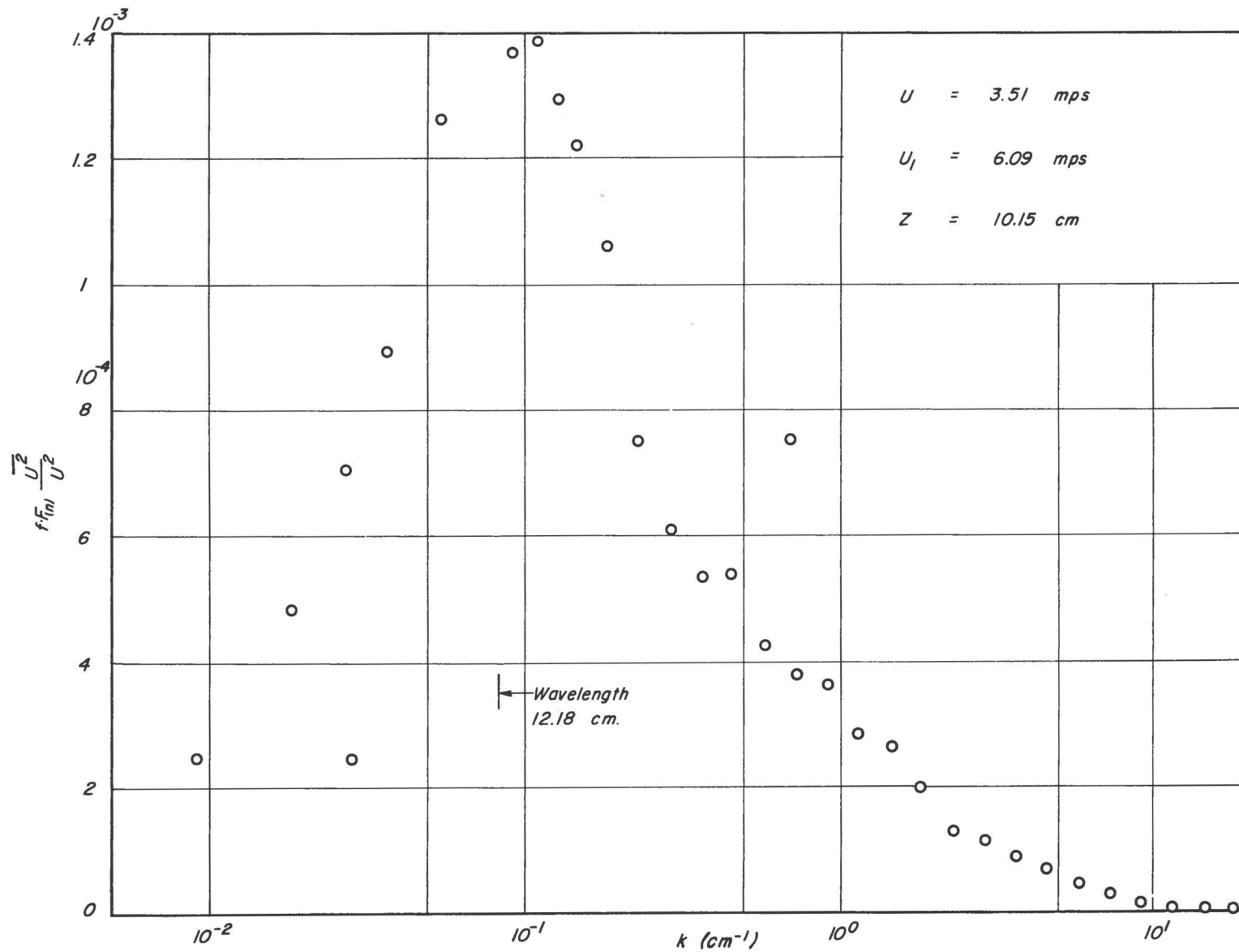
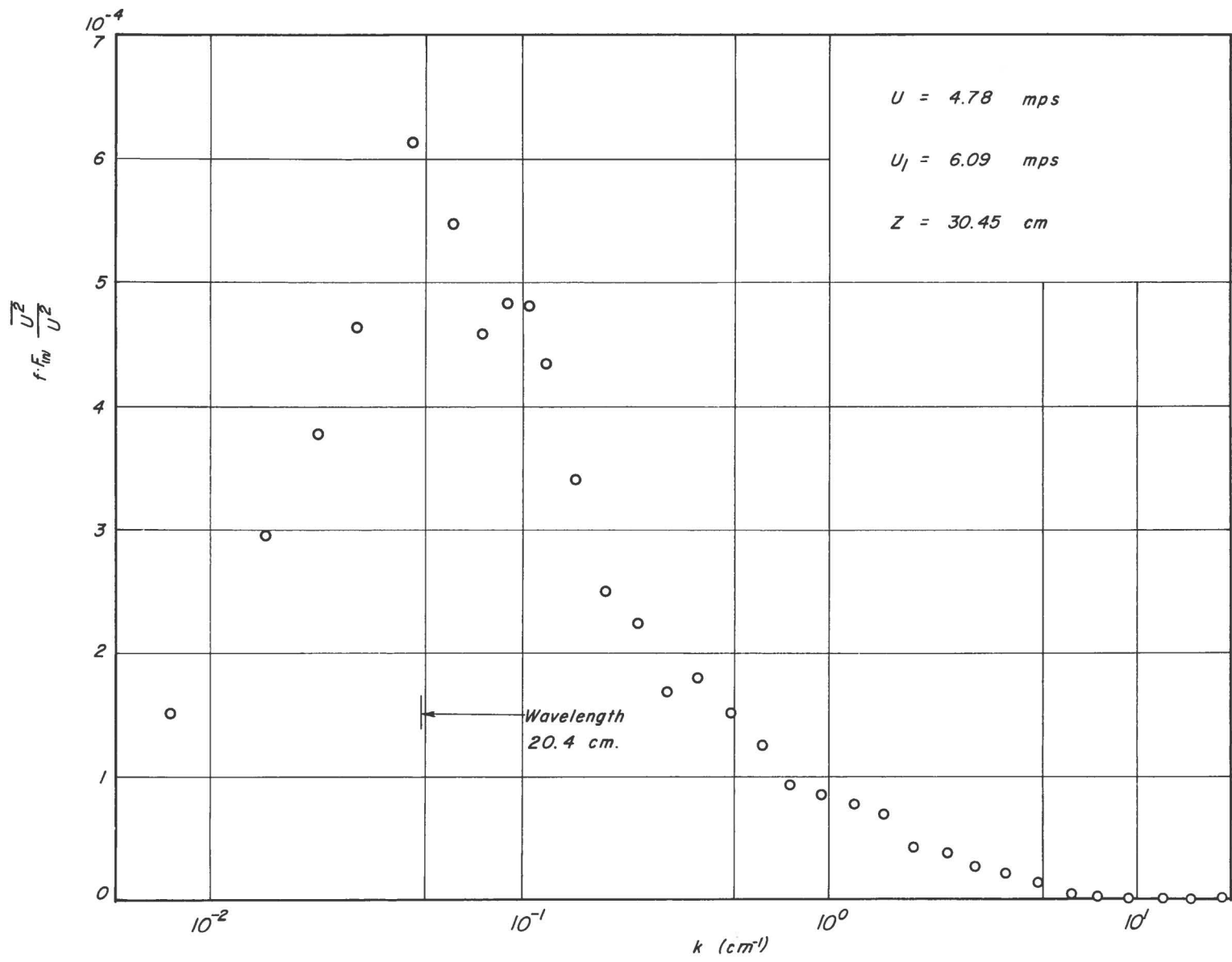


Fig. 22a Evaluation of the large scale turbulence

Fig. 22b Evaluation of the large scale turbulence



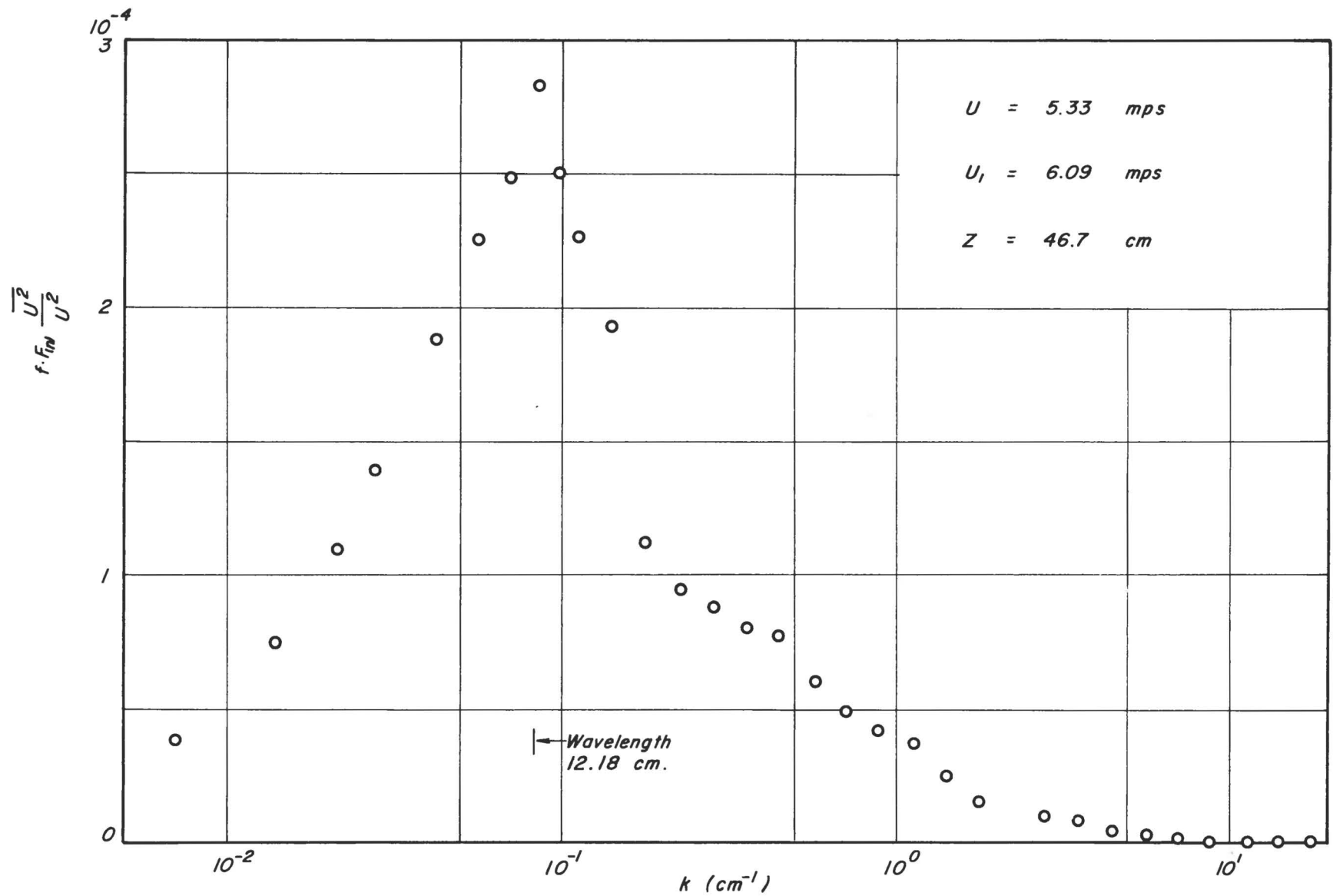


Fig. 22c Evaluation of the large scale turbulence

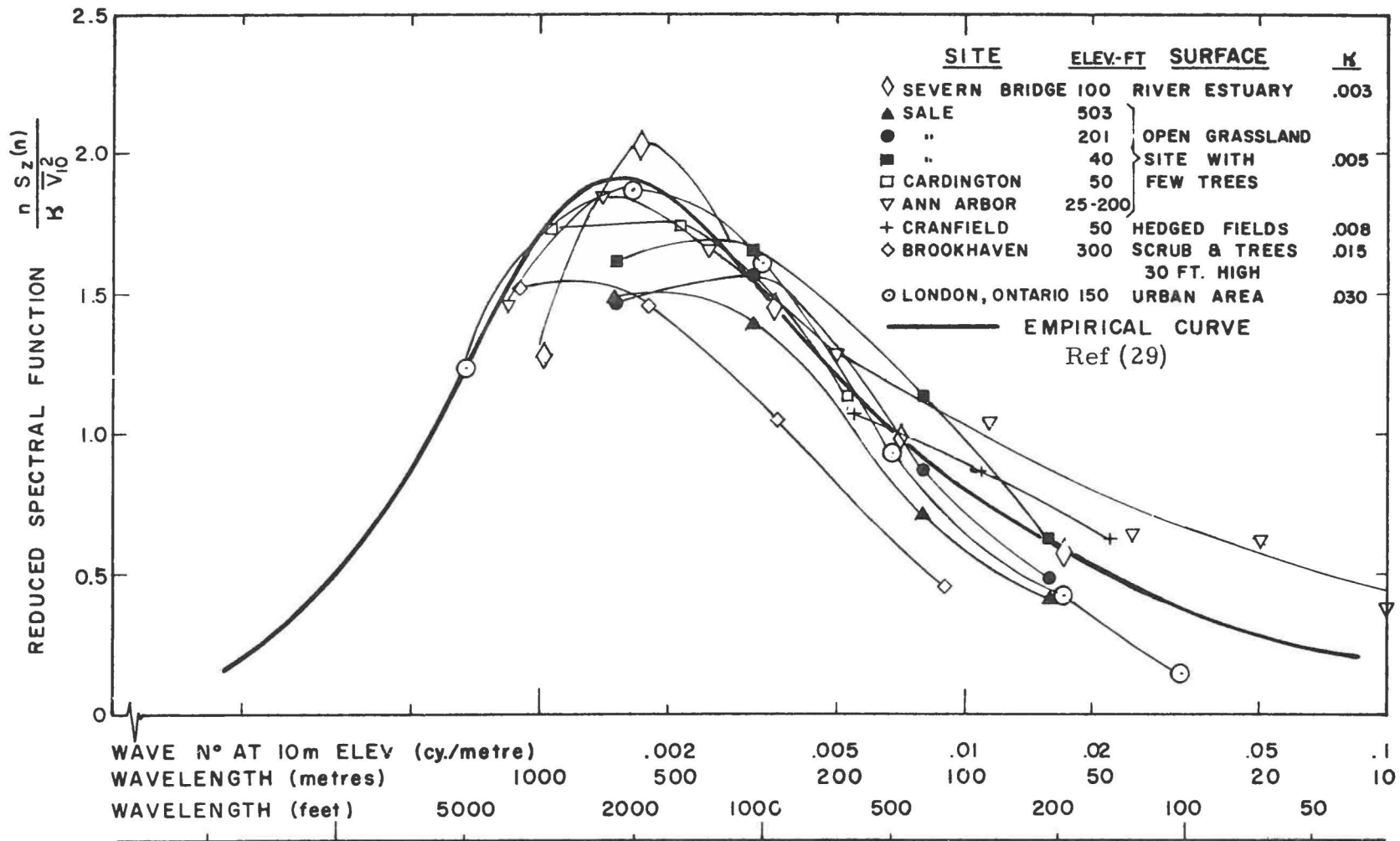


Fig. 23 Spectrum of horizontal gustiness in high winds

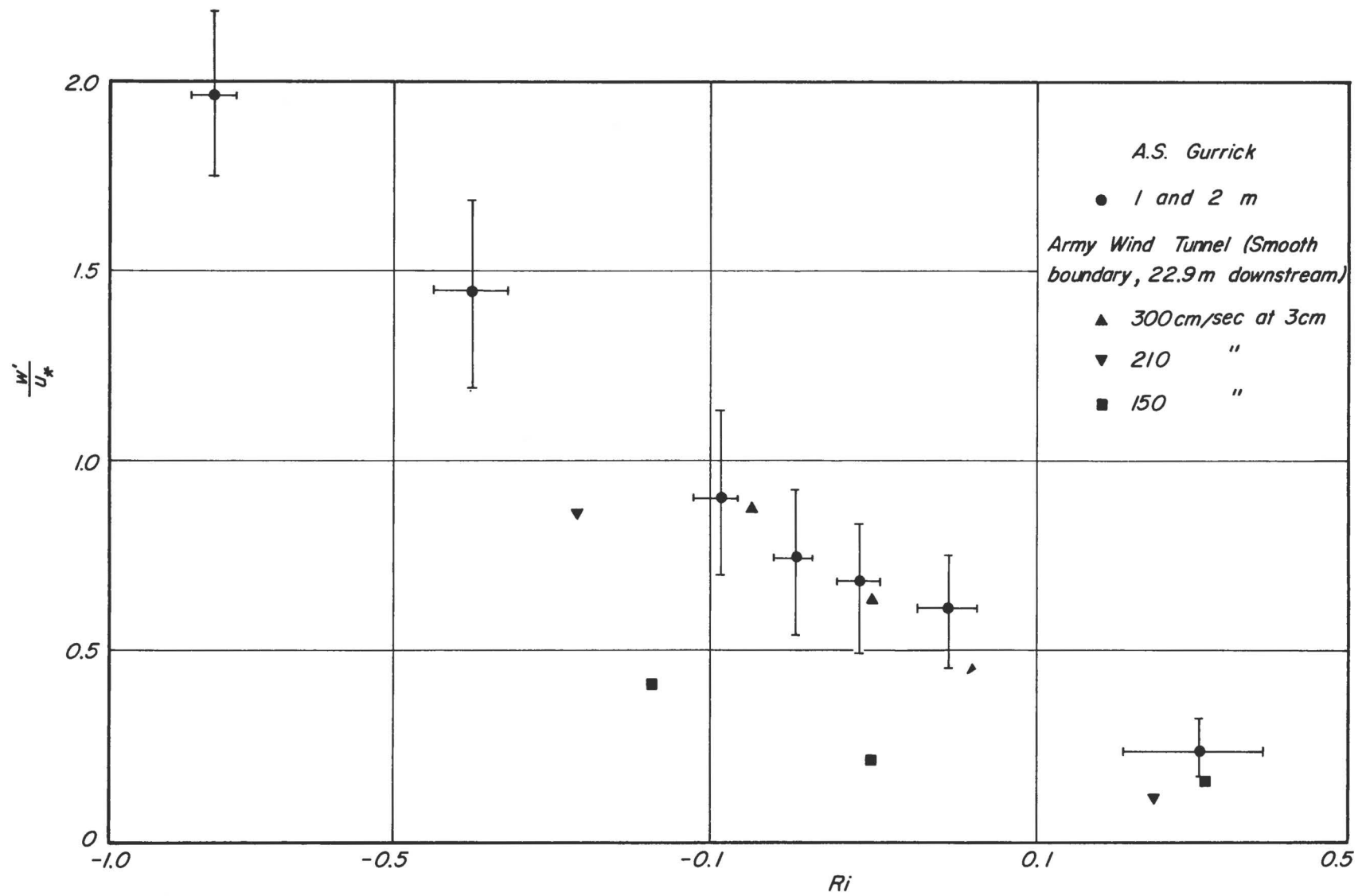


Fig. 24 Turbulent intensity of vertical velocity component versus Richardson number

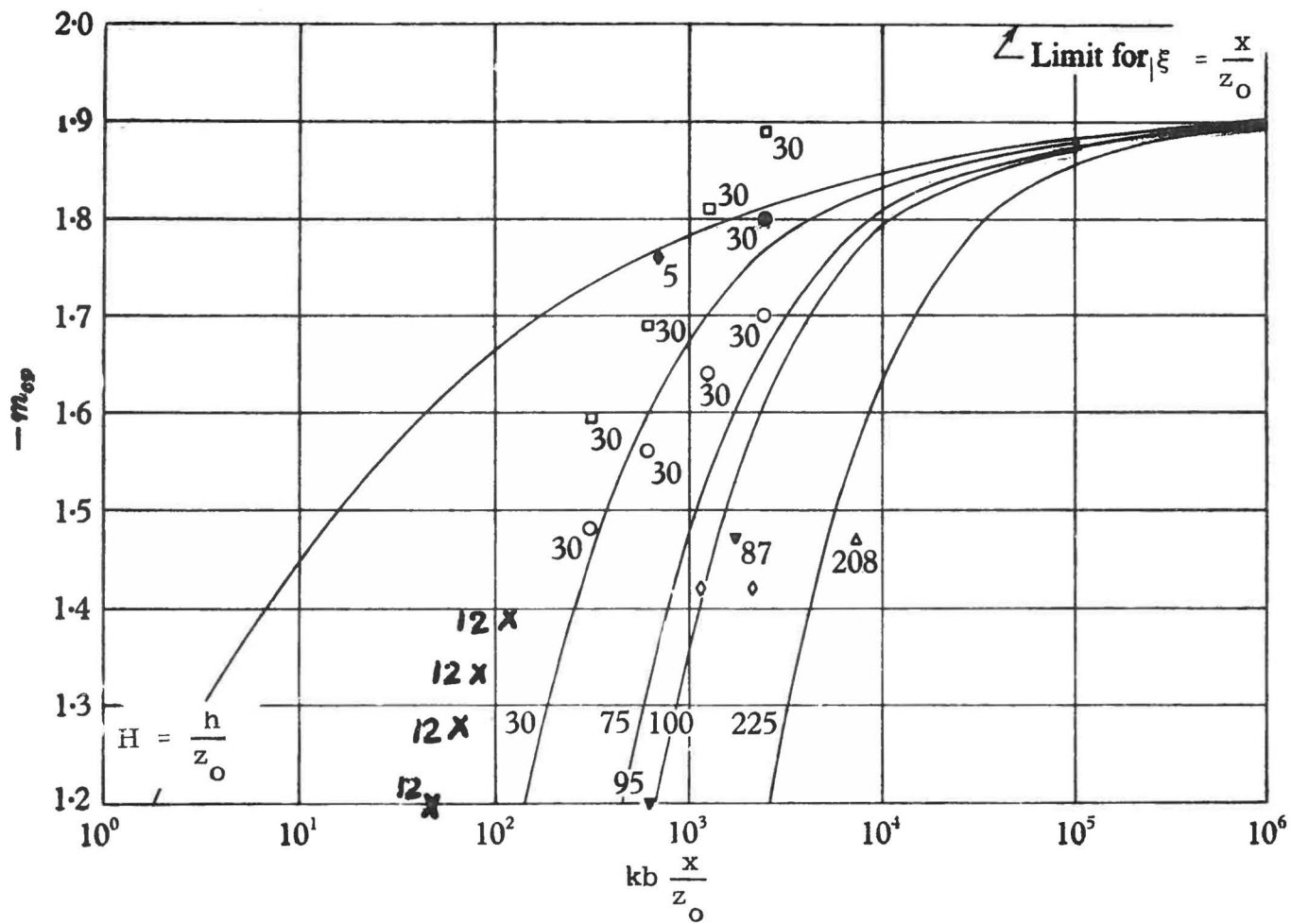


Fig. 25 The exponent-of-distance  $m_{cp}$  for attenuation of maximum ground-level concentration as a function of distance and source height resulting from a point source in a neutral boundary layer.

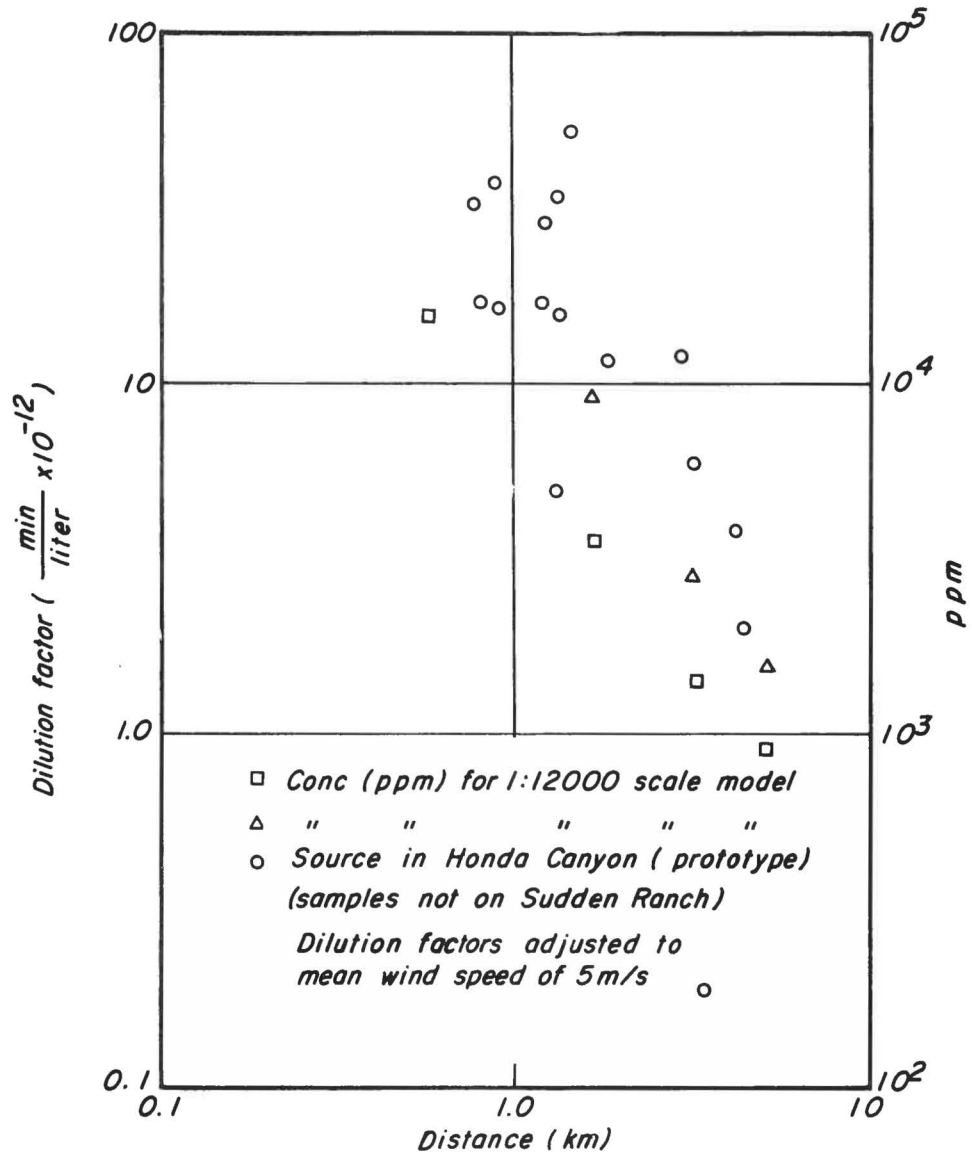


Fig. 28 Downwind variation of dilution and concentration